STUDIES OF ISOTOPE EFFECTS IN FISSION-PRODUCT RARE GASES

STUDIES OF ISOTOPE EFFECTS IN FISSION-PRODUCT RARE GASES

by

WILLIAM BRIAN CLARKE, B.A.

A Thesis

Submitted to the Faculty of Graduate Studies

in Partial Fulfilment of the Requirements

for the Degree

Doctor of Philosophy

McMaster University
September 1962

DOCTOR OF PHILOSOPHY (1962)
Physics

McMASTER UNIVERSITY
Hamilton, Ontario

TITLE: Studies of Isotope Effects in Fission-Product Rare Gases

AUTHOR: William Brian Clarke, B.A. (Trinity College, Dublin)

SUPERVISOR: Professor H. G. Thode

NUMBER OF PAGES: xi, 120

SCOPE AND CONTENTS: Part I describes a series of experiments concerning the diffusion of fission-product rare gases from uranium oxides, and other uranium compounds. Abnormal enrichments in Xe^{131} and Xe^{132} were found in low temperature fractions of xenon evolved from some of the oxide powders. The results for U_3O_8 are in agreement with the earlier work of Kennett and Thode in this laboratory. The isotope enrichments in Xe^{131} and Xe^{132} are explained in terms of a sphere model for diffusion, and concentration of xenon precursors in regions of low activation energy. Direct experimental evidence is given for the concentration of fission-product iodine in regions of low activation energy.

Part II gives the results of isotopic analyses of rare gases from stone meteorites, the atmosphere and natural gas. The analyses revealed the presence of fission-product xenon in the atmosphere (possibly from spontaneous fission of Pu^{244} in the early history of the earth) and also fission-product xenon (from spontaneous fission of U^{238}) in natural gas. Fission yield discrepancies at Xe^{131} and Xe^{132} for fission-product xenon in the atmosphere and in natural gas are explained by analogy with the results of Part I.

ACKNOWLEDGEMENTS

I would like to express my sincere appreciation for the encouragement and inspiration given by Dr. H. G. Thode throughout the course of this work. I would also like to thank Dr. Hitoshi Sakai, Dr. Makoto Shima, and Dr. C. C. McMullen who contributed many valuable suggestions.

The completion of this work has been made possible by generous scholarships from McMaster University and Eldorado Mining and Refining, Limited.

I am also indebted to Dr. R. H. Betts and Dr. R. G. Hart of Atomic Energy of Canada Limited for supplying the uranium oxide samples, and Dr. H. Faul of the U. S. Geological Survey and Mr. H. P. Wheeler, Jr. of the U. S. Bureau of Mines for supplying the natural gas samples.

TABLE OF CONTENTS

LIST OF TABLES

LIST OF ILLUSTRATIONS

PART I

ISOTOPE EFFECTS IN THE DIFFUSION OF FISSION-PRODUCT RARE GASES FROM URANIUM OXIDES AND OTHER URANIUM COMPOUNDS

I. INTRODUCTION

The fission process in uranium results in the production of krypton and xenon (Thode and Graham 1947; Yaffe and Macintosh 1947). The average total yield of krypton and xenon isotopes is approximately 25%, that is, one in every eight fission-product atoms is a rare gas atom. The xenon-krypton ratio is about 6 to 1, with Kr^{85}, the radioactive isotope of long half-life ($T_{1/2}$ = 10.27 y), making up about 1% of the total krypton and xenon. The fission gas must be accommodated in the fissile material, either dissolved in the lattice structure or enclosed in grain boundaries or microcracks. A recent study of diffusion of fission gas from U_3O_8 by Kennett and Thode (1960) revealed remarkable isotope effects for fission-product xenon released at low temperatures. This work was undertaken in order to examine these isotope effects in various systems and to obtain experimental evidence for a mechanism.

In the last twenty years, nuclear reactors, which use the energy liberated in fission of heavy elements, have become increasingly important. The present supplies of coal, oil, gas and water as sources of power are not inexhaustible, and there is no certainty that scientists will be able to control the fusion process and use it as a source of power. At the present time, however, nuclear reactors are not competitive in an economic sense with conventional forms of power. The capital investment of building a nuclear reactor is high and so are the running costs.

Canada has concentrated her efforts on natural uranium, heavy-water-moderated reactors. The uranium is in the form of uranium dioxide as a high density sinter. The use of uranium dioxide in this form has many advantages. It is highly resistant to corrosion by water, and this is an important feature if, by some mishap, the fuel should come into contact with the moderator. Uranium dioxide fuel can withstand high burnup, such as 10,000 megawatt days per ton, without undue swelling. At high values of burnup the oxide fuel retains fission-product gases remarkably well and this allows the gap between the fuel element to be kept low, and thus minimise the neutron wastage. A major disadvantage is the very low thermal conductivity, which causes a large heat gradient across the fuel element. The centre of the fuel element in some cases reaches a temperature of about 1600°C, and plastic flow and cracking can occur.

Since 1955, several studies have been made on the ability of uranium dioxide to retain fission-product rare gases. These studies may be divided into two main types. The first type of experiment is performed in the reactor core as described by Markowitz et al (1956). The fission gases are swept by means of helium from the surface of specimens of UO_2 within a furnace located in the reactor core to a charcoal trap. Subsequently, the rare gases are analysed by gamma spectrometry. In the second type of experiment, samples of UO_2 are irradiated, transferred to a furnace, and heated at various temperatures. The evolved rare gases are collected in a charcoal trap and analysed by gamma spectrometry. Such experiments have been performed at elevated temperatures (900°C - 1600°C) by Booth and Rymer (1956, 1958). Their experiments showed that the escape of Xe^{133} ($T_{1/2}$ = 5.3 d) and Kr^{85} ($T_{1/2}$ = 10.27 y) could be interpreted on the basis of a simple model in which the UO_2 sinter is considered to be an

assembly of hypothetical spheres. Similar experiments on fission-product rare gas diffusion in UO_2 have been carried out by other investigators and there exists in the literature a wide range of values for diffusion coefficients and activation energies for diffusion (for a review see Lewis 1960).

It appears that a slight excess of oxygen above the stoichiometric $UO_{2.0}$ affects the diffusion of rare gases through the lattice to a marked degree. Lindner and Matzke (1959) studied the diffusion of Xe^{133} in uranium oxides of varying oxygen content and found there was a striking increase of the diffusion constant with increasing oxygen content from $UO_{2.00}$ to $UO_{2.12}$. A similar behaviour had been noted by Belle (1959) for the diffusion of oxygen in UO_2. Lindner and Matzke suggested that there might be a relation between the autodiffusion of oxygen and the diffusion of fission-product rare gases in UO_2.

Recently, Kennett and Thode (1960) approached the problem in a different way. They determined the volume and isotopic composition of krypton and xenon evolved from neutron-irradiated U_3O_8 powder as a function of temperature in the temperature range 30°C - 1200°C. The data showed that the abundances of Xe^{131} and Xe^{132} did not remain constant relative to Xe^{136}, but showed remarkable enrichments in the gas fractions evolved at temperatures below 500°C. The krypton samples showed no observable deviation from the normal isotope pattern observed for krypton from the thermal neutron fission of U^{235}.

Kennett and Thode also noted that there were two activation energies for the xenon diffusion process. Below 410°C, an activation energy of 3 k cal/mole was predominant and above 410°C, an activation energy of 39 k cal/mole was predominant. Since the isotope enrichments

were observed in the low temperature region, Kennett and Thode suggested that at these temperatures the rate-controlling process was diffusion from surfaces of particles or from grain boundaries. The abnormal isotope enrichments in xenon could be explained by a concentration of xenon precursors (i.e. iodine, tellurium, etc.) on the surfaces of particles or in the grain boundaries. This suggestion seems reasonable since Xe^{131} and Xe^{132} have long-lived precursors, unlike Xe^{134} and Xe^{136}. Also, the absence of abnormal isotope effects for krypton could be explained by the fact that the krypton isotopes chiefly produced in fission have short-lived precursors.

The purpose of the work reported in Part I of this thesis may be summarised as follows:

1. To confirm the earlier results of Kennett and Thode.
2. To obtain data for the radioactive isotopes of xenon.
3. To examine the isotope effects in various systems.
4. To obtain direct experimental evidence of the concentration of precursors of xenon in regions of low activation energy.

II. EXPERIMENTAL

A. SAMPLE PREPARATION

1. Preparation and Use of Tracers

The isotope dilution method consists of adding a calibrated amount of an element of known isotopic composition (referred to as the "spike", or "tracer") to an unknown amount of the same element, which must be of different isotopic composition. If the isotopes present in the tracer do not occur in the unknown sample, then one mass spectrometric analysis of the tracer-unknown mixture serves to determine the unknown amount, as well as its isotopic composition. If the isotopes present in the tracer do occur in the unknown sample, then two mass spectrometric analyses are necessary, one to determine the isotopic composition of the unknown sample, and the other to determine the isotopic composition of the tracer-unknown mixture.

The tracer used for krypton and xenon determinations was a mixture of pure Kr^{80}, Kr^{82} and Xe^{128}, obtained by irradiating KBr and KI in the reactor. The krypton-xenon tracer supply was stored in a five-litre reservoir connected to gas pipettes. The method of gas pipetting and calibration of the tracers has been described in a previous thesis by Young (1958).

Since the isotopes present in the krypton-xenon tracer occur only to a negligible extent, compared to the other isotopes of krypton and xenon formed in fission (Kennett and Thode 1956), one mass spectro-

metric analysis of the tracer-fission gas mixture was sufficient to determine the amount and isotopic composition of krypton and xenon in fission gas samples.

2. Preparation of Powders

a. Uranium Oxides

U_3O_8 was prepared by heating uranyl nitrate in air at 750°C. The other uranium oxides used in this work were obtained in the form of compact sinters from Atomic Energy of Canada Limited. These oxides had the following compositions: $UO_{2.005}$, $UO_{2.175}$ and $UO_{2.241}$.

The oxides were crushed and sieved and the fraction between 200 mesh and 325 mesh was retained for irradiation. All the samples except U_3O_8 were crushed and sieved in an argon atmosphere in order to avoid possible reaction of the oxides with oxygen present in the air.

b. Uranium Hydride

Finely-divided UH_3 powder was prepared by heating uranium filings in an atmosphere of hydrogen at 225°C. The hydrogen was prepurified by passing through a copper-wool trap at 650°C, and also through a magnesium perchlorate drying train. The uranium filings were washed with nitric acid to remove surface oxide.

c. Uranium Nitride

Uranium nitride powder was prepared by heating UH_3 powder in an atmosphere of ammonia at 200°C.

3. Extraction of Fission Products from Neutron Irradiated Powders

a. Extraction of Stable Krypton and Xenon

A quartz vial, containing the neutron irradiated powder, was placed in the sample furnace as shown in Fig. I-1. After the system had been pumped out, the vial was broken and fission gas, which had escaped

FIG. I-1

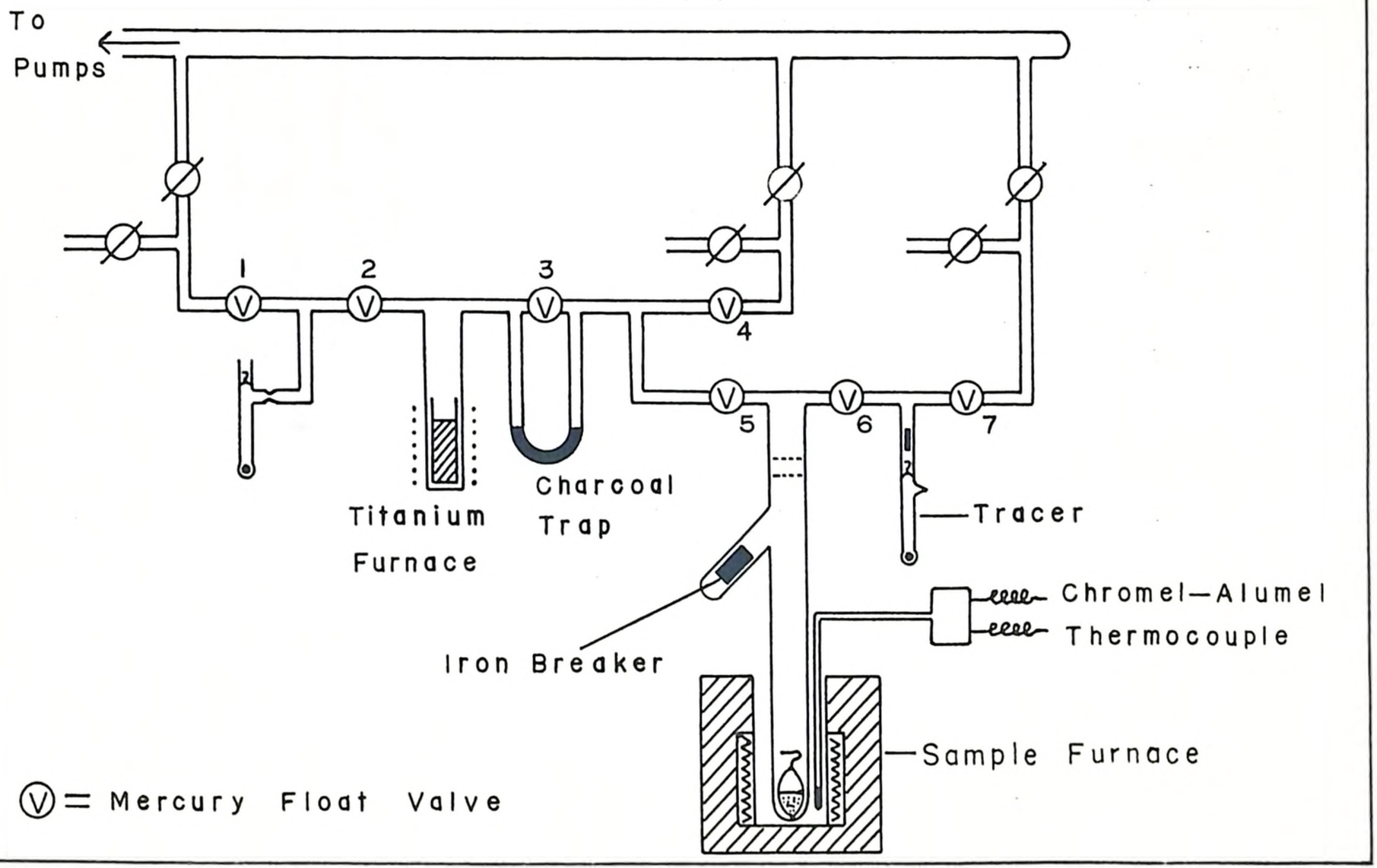

RARE GAS EXTRACTION & PURIFICATION SYSTEM

from the powder during irradiation or since irradiation, was collected in the charcoal trap at liquid nitrogen temperature. The gas was then purified in the titanium furnace, which was heated to 800°C, transferred to the sample tube and removed. The sample furnace temperature was then raised to about 100°C and a krypton-xenon tracer admitted to the furnace section, with mercury float valves V_5 and V_7 closed and V_6 open. The temperature of the furnace was held constant for 3 hours, and during this time the tracer was allowed to mix with the fission gas evolved from the powder. During the final 10 minutes of the heating period the tracer-fission gas mixture was collected in the charcoal trap, held at liquid nitrogen temperature. The gas was then purified in the titanium furnace, collected in a sample tube and removed for analysis.

The above procedure was repeated at temperature intervals of about 150°C, from 100°C to 1100°C. The isotopic composition, as well as the amount of fission-product krypton and xenon evolved at each constant temperature heating period, was determined by subsequent mass spectrometric analysis of the tracer-fission gas mixtures.

b. Extraction of Radioactive Xenon from U_3O_8

The apparatus shown in Fig. I-1 was used to obtain temperature fractions of Xe^{133} ($T_{1/2}$ = 5.27 d) and Xe^{135} ($T_{1/2}$ = 9.2 h) from neutron irradiated U_3O_8 powder. All the steps in the procedure described in the previous section were carried out except that the krypton-xenon tracer was replaced by a sample tube containing about 1 cc STP of stable xenon. This ensured complete collection of radioactive xenon evolved from the U_3O_8 powder during each constant temperature heating period. Sample tubes containing a mixture of Xe^{133} and Xe^{135} were removed for analysis. The

analysis was carried out by gamma-counting with a NaI (Tl) scintillation detector and a 256 channel pulse height analyser. Xe^{133} was detected by means of its 81 kev γ-ray and Xe^{135} by means of the 248 kev γ-ray of Cs^{135}. The geometry of the samples with respect to the NaI crystal was reproduced closely for each sample.

c. Extraction of Radioactive Iodine and Xenon from U_3O_8

The apparatus used to obtain temperature fractions of radioactive iodine and xenon from irradiated U_3O_8 is shown in Fig. I-2. Sample tubes S_1, S_2 .... etc. each contained a few milligrams of stable iodine and about 1 cc STP of stable xenon. The system could be sealed at points indicated by dashed lines in the diagram. The iron breakers were encased in pyrex in order to avoid possible loss of iodine on the iron surfaces.

After the system had been pumped out, the line was sealed at A, and the temperature of the furnace raised to about 100°C. The tip of the quartz vial containing the irradiated U_3O_8 powder, and the break-seal of S_1 were then broken. The furnace temperature was maintained constant during the next 3 hours, and during this time the stable iodine was mixed with the radioactive iodine evolved from the powder by periodic heating of the extraction system (with a large flame) to about 200°C. At the end of the 3-hour sample heating period, dry ice (-80°C) was placed on T, and liquid nitrogen (-185°C) was placed on the charcoal trap. The extraction system was then heated to about 200°C, and break-seal B was broken. After a few minutes, condensation of iodine in T was complete, as judged from the disappearance of a characteristic discharge colour in the extraction system. The line was then sealed at C and the above procedure repeated for a sample temperature of about 250°C. The charcoal trap

FIG. I-2

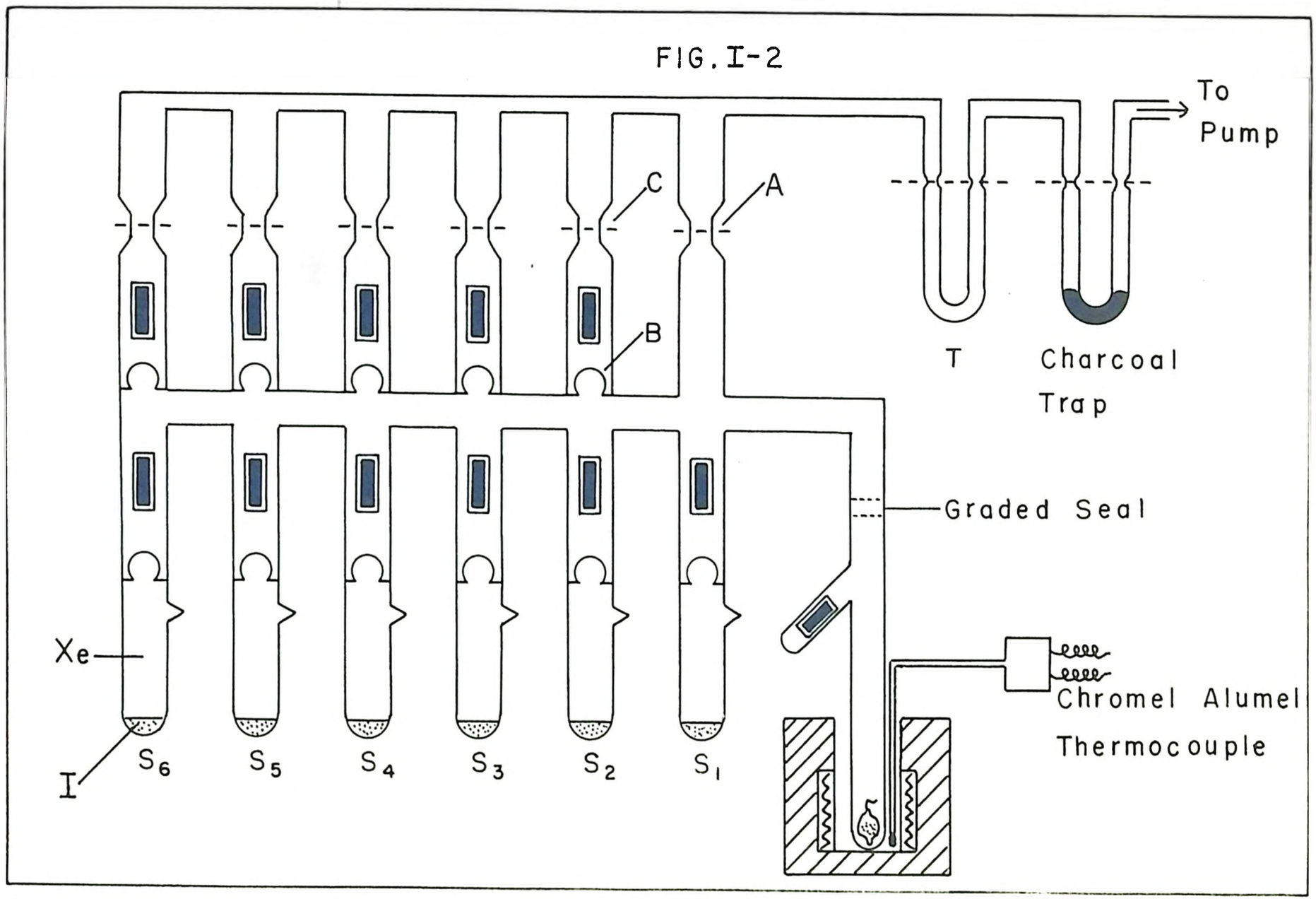

EXTRACTION SYSTEM FOR I^{131} AND Xe^{133}

and T were sealed off and removed for subsequent analysis by the method described in the previous section. I^{131} ($T_{1/2}$ = 8.05 d) was detected by means of its 364 kev γ-ray, and Xe^{133} was detected as described in the previous section.

B. MASS SPECTROMETRY

1. The Mass Spectrometer

The mass spectrometer used throughout this work was designed specifically for isotope abundance measurements on small rare gas samples. Fig. I-3 shows the essential parts of the apparatus. The ion optics of the machine are of conventional first-order direction-focusing type. Source and collector slit widths of 0.1 mm, and 0.3 mm, respectively, and an orbit radius of 10 in, provided a resolving power of 620. This was found to be sufficient to separate cleanly krypton and xenon isotopes from isobaric hydrocarbons present either as impurities in the sample or as instrumental background.

The ion detector was a 9-stage electron multiplier with Cu-Be dynodes. The initial gain of the multiplier, after it was activated by heating in hydrogen, was found to be 3×10^5 for interdynode potentials of about 300 V. During a year of continuous operation the gain fell to a permanent value of 4×10^4.

2. Methods of Sample Introduction

In this work two methods of introducing the rare gas samples into the ion source were employed. In the conventional flow method the sample was allowed to leak into the ion source at a steady rate and was continuously removed by the pumps. In the static method the rare gas sample was expanded into the mass spectrometer volume which had been completely sealed off from the pumps.

FIG. I-3

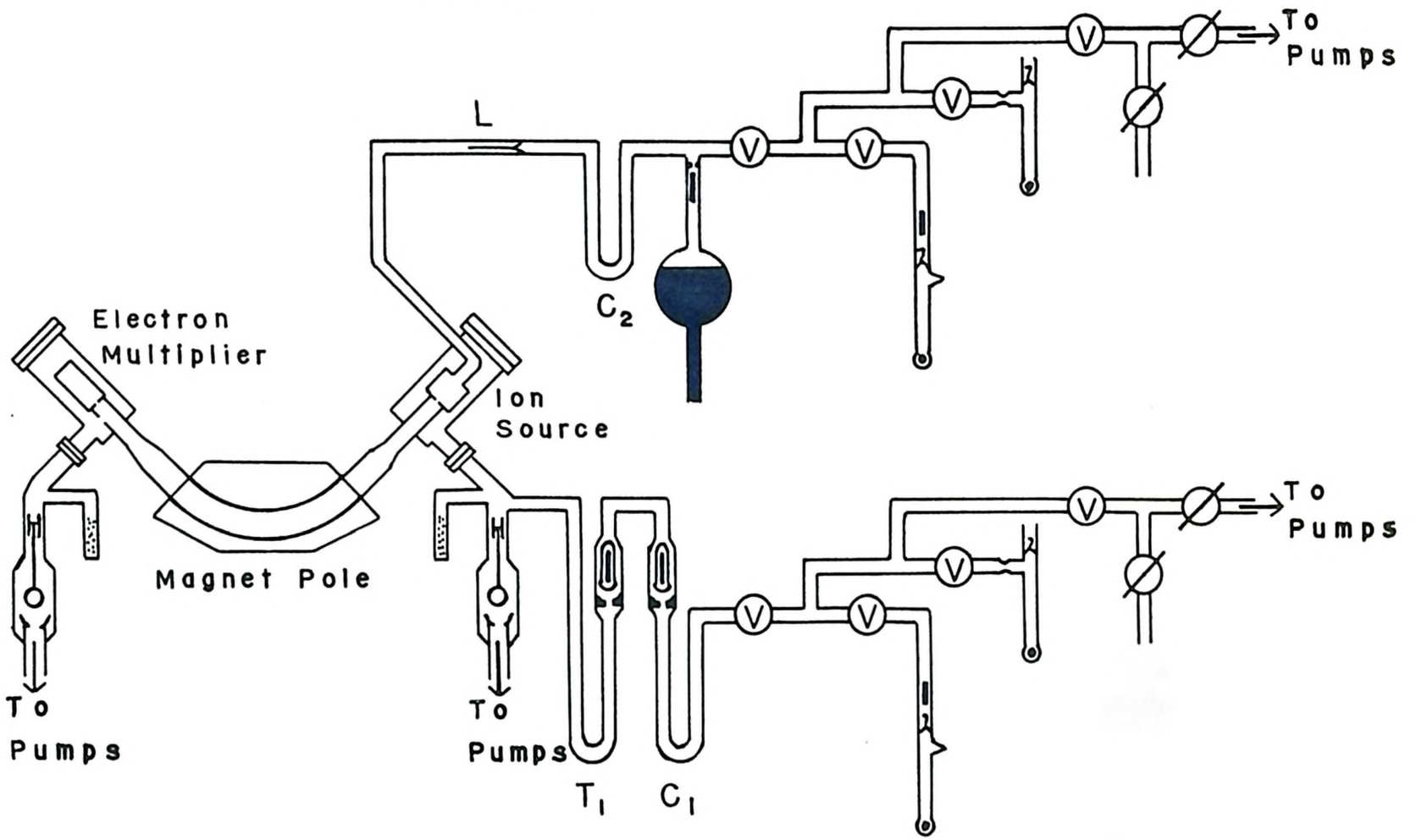

MASS SPECTROMETER AND SAMPLE INLET SYSTEMS

a. The Flow Method

The gas was allowed to flow from the sample-handling system through the capillary leak L (Fig. I-3) into the ion source. Liquid nitrogen was placed on the capillary trap C_2 before the sample containing a mixture of krypton and xenon was introduced. In this way the xenon was condensed in the trap and held there during krypton analysis.

During a flow analysis the isotopic composition of the sample will change with time since the light isotopes diffuse faster through the leak than the heavy isotopes. This effect could become important if an appreciable fraction of the sample had passed through the leak during a flow analysis. The size of the capillary leak used was such that about ten per cent of the sample enclosed in the minimum volume of the sample-handling system passed through the leak during 30 minutes of analysis. No systematic change in isotope ratios which could be attributed to mass fractionation in the leak was observed during this period of time.

By means of the flow method, about 10^9 atoms of any isotope of krypton or xenon could be detected. An estimate of the sample size necessary for convenient analysis would be 10^{10} atoms per isotope.

b. The Static Method

In this method the mass spectrometer volume was isolated from the pumps and a small rare gas sample then expanded into the sealed-off system. The static method was found to have a considerable advantage in sensitivity over the flow method. Ion currents from a sample of rare gas introduced into the isolated system were approximately 2000 times greater than ion currents from a sample of the same size analysed under flow conditions.

A leakproof valve, which could be baked at high temperatures, and opened or shut by means of two small hand magnets, is shown in Fig. I-4. Two such valves were incorporated in the pumping leads of the mass spectrometer. Two quartz thimbles, each containing a few grams of titanium sponge, were sealed on to the pumping leads above the valves as shown in Fig. I-4. The thimbles were heated to 800°C and at this temperature the hot titanium served as a "getter", removing gases other than rare gases (CO for the most part) released as a result of slight outgassing of the system. A residual pressure of 5×10^{-8} mm Hg could be maintained in the sealed-off system for several hours. The hydrocarbon background in the instrument was not observed to increase during this period of time.

Liquid nitrogen was placed on the capillary trap C_1 (Fig. I-3) before introduction of the sample. In this way the krypton was admitted to the isolated system and, during krypton analysis, the xenon was retained. The krypton was pumped away after analysis and the xenon then admitted by raising the trap temperature to -80°C. During analysis of krypton and xenon, the traps C_2 and T_1 were held at -80°C. In this way the leakage of mercury from the sample-handling system into the isolated mass spectrometer was kept at a minimum.

3. Systematic Errors in Isotope Abundance Measurements

a. Mass Discrimination

Several of the mass spectrometer components, including the gas leak, the ion source, and the electron multiplier, may introduce mass dependence into isotope abundance measurements. The mass discrimination of the instrument, operating under both flow and static conditions, was checked frequently during the course of this work. This was done by the

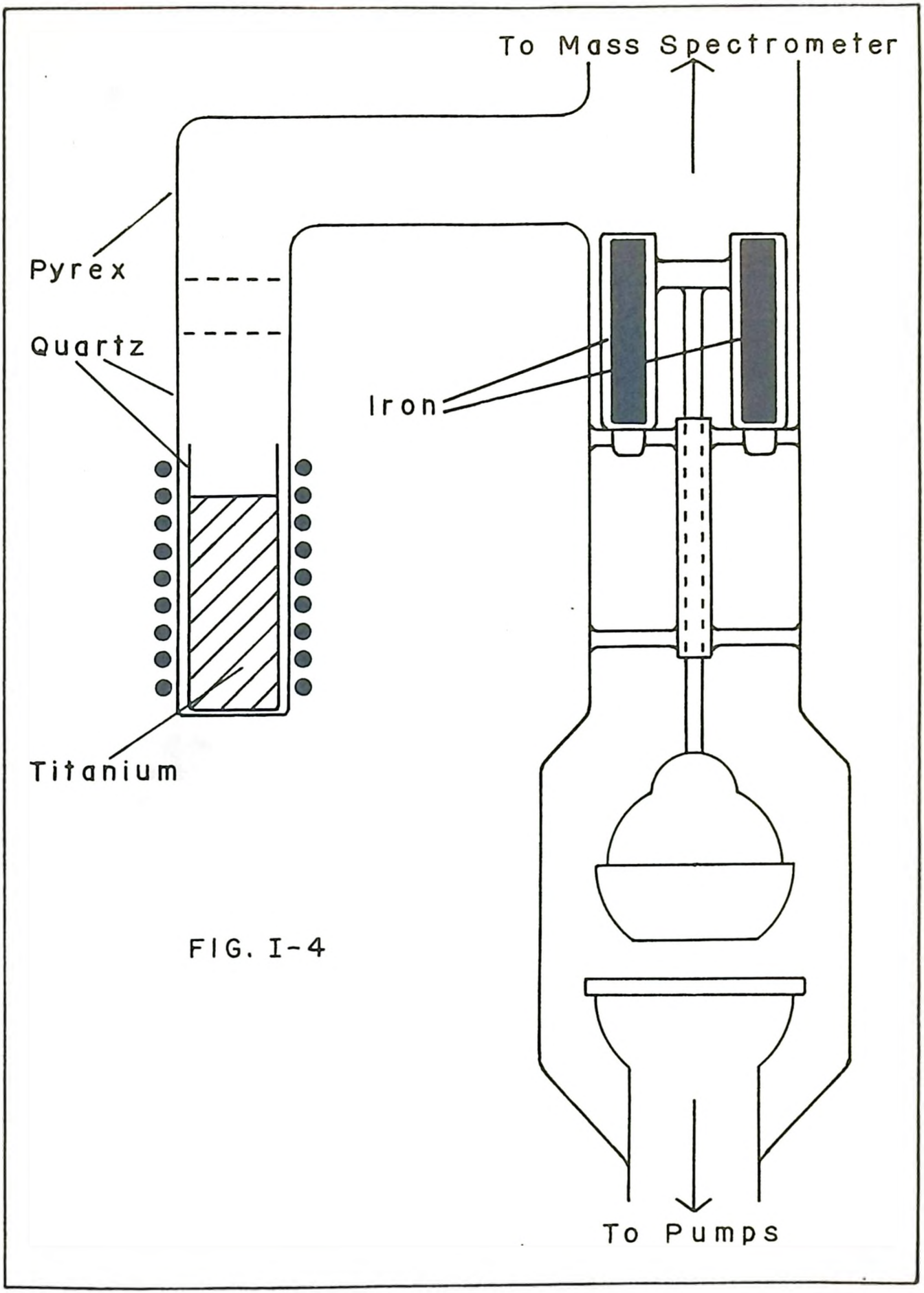

FIG. I-4

MASS SPECTROMETER VALVE AND TITANIUM FURNACE

analysis of samples of krypton and xenon obtained from air by the purification techniques described previously, and the results compared with the accepted values for the isotopic abundances of atmospheric krypton and xenon given by Nier (1950).

Isotope abundance measurements on atmospheric krypton and xenon, analysed by the flow method, and atmospheric xenon, analysed by the static method, were found to agree with the accepted values given by Nier, within the standard deviation of the measurements (about 0.3%). When the measured isotopic abundances of atmospheric krypton, analysed by the static method, were compared with the accepted values, a linear deviation was noted. This deviation favoured the 80/86 ratio by about 2% and was attributed to instrumental mass discrimination. A correction was therefore applied to all isotope abundance measurements on krypton analysed by the static method.

b. Memory Effect

During this work it was found that isotope abundance measurements on a sample of krypton or xenon could be altered significantly by "memory effect", that is, contamination of a sample being analysed by the remnant of a sample, of different isotopic composition, which had been previously analysed in the instrument.

It was found that memory from a previous sample could be greatly reduced by baking the instrument at about 300°C for 12 hours, during which time the ion source filament was kept on and the ion source was continuously flushed with either neon or argon, admitted via the capillary leak. Xenon from the previous sample, which had condensed in the mass spectrometer liquid air traps, was removed by warming the traps to -80°C

for about 30 minutes. During the final hour of the baking period, the ion accelerating voltage was switched on and the resulting beam of neon or argon ions was scanned slowly across the mass spectrometer tube. In this way, traces of the previous sample imbedded in the tube walls, or in the collector assembly, were removed to a large extent.

III. RESULTS

A. DIFFUSION OF STABLE KRYPTON AND XENON FROM IRRADIATED URANIUM OXIDES

1. Isotopic Effects

A description of the oxide samples and pertinent irradiation details is given in Table I-I. All the oxide samples were irradiated in the McMaster reactor. The $UO_{2.175}$ and $UO_{2.241}$ samples were irradiated continuously at approximately constant neutron flux. The operation of the reactor was on a 16-hour day, 5-day week basis during the irradiation of the U_3O_8 and $UO_{2.005}$ samples. The listed values for thermal neutron flux were obtained from quarterly progress reports of the McMaster reactor. The flux values are probably accurate to 10%.

During mass spectrometric analyses of the tracer-fission gas samples evolved from the irradiated powders, it was found that some of the rare gas samples contained appreciable amounts of krypton and xenon of atmospheric origin. Since the long-lived I^{129} prevents the formation of Xe^{129} in young fission products, and the independent yield of Xe^{129} in thermal neutron fission of U^{235} is negligible, any Xe^{129} observed in the tracer-fission gas samples was assumed to be due to atmospheric contamination, and a correction was applied to the xenon isotope pattern where necessary. The yields in thermal neutron fission of U^{235} of the isotopes Kr^{80} and Kr^{82} were also assumed negligible (Kennett and Thode 1956). The krypton isotope pattern was corrected for atmospheric contamination where necessary by observing a change in the Kr^{80}/Kr^{82} ratio in the tracer-fission gas samples relative to the Kr^{80}/Kr^{82} ratio in the tracer reservoir.

TABLE I-I

Description of the Uranium Oxide Samples and Irradiation Details

Sample	Sample Weight gms	Particle Size Range	Thermal Neutron Flux neut/cm^2/sec	Irradiation Time Hours	Cooling Time
U_3O_8 I	1.60	200-325 mesh	1.4×10^{13}	100	20 months
U_3O_8 II	1.80	200-325 mesh	1.4×10^{13}	100	10 days
U_3O_8 III	1.60	200-325 mesh	1.4×10^{13}	100	21 days
$UO_{2.005}$	1.74	200-325 mesh	1.4×10^{13}	100	8 months
$UO_{2.175}$	1.67	200-325 mesh	1.2×10^{13}	100	8 months
$UO_{2.241}$	1.60	200-325 mesh	1.2×10^{13}	100	8 months

The results of the mass spectrometric analyses of krypton and xenon evolved from U_3O_8 I at various temperatures are given in Tables I-II and I-III. All isotopic abundances of krypton are given normalised to $Kr^{86} = 1.000$. The abundance of Kr^{85} ($T_{1/2} = 10.27$ y) has been corrected for decay between irradiation and analysis. For comparison are given the relative fission yields of the krypton isotopes (expected abundances) in the thermal neutron fission of U^{235} (Wanless and Thode 1955). The xenon isotope abundances are normalised to Xe^{136}, with a value of 1.000 for the cumulative abundance of Xe^{134}. The fission yields of Xe^{131} and Xe^{132} (relative to Xe^{134}) are given for comparison. Wanless and Thode give a value of 0.803 for the fission yield of Xe^{136} relative to the fission yield of Xe^{134}. The marked increase in apparent fission yield of Xe^{136} is due to neutron capture in Xe^{135} during irradiation. Also given in Tables I-II and I-III are the expected amounts of fission-product krypton and xenon produced. The following formula was used:

$$N_i = N_{U235}\, \phi\, t\, \sigma_f\, Y_i$$

where N_i is the number of atoms of krypton or xenon produced

N_{U235} is the number of atoms of U^{235} in the powder sample

ϕ is the thermal neutron flux in neutrons/cm^2/sec

t is the irradiation time in seconds

σ_f is the cross-section for thermal neutron fission of U^{235}

and Y_i is the fractional yield of the stable krypton or xenon isotopes in thermal neutron fission of U^{235}.

TABLE I-II

The Isotopic Composition and Amount of Fission Product Krypton Evolved from U_3O_8 I (Cooling Time = 20 Months) as a Function of Temperature

Temperature Plateau °C	Isotope				Krypton Atoms Released	Cumulative Krypton Atoms Released
	83	84	85	86		
140	0.276	0.505	0.148	1.00	4.52×10^{11}	4.52×10^{11}
250	0.270	0.500	0.148	1.00	3.43×10^{11}	7.95×10^{11}
380	0.276	0.510	0.147	1.00	1.08×10^{12}	1.88×10^{12}
570	0.276	0.500	0.142	1.00	4.69×10^{12}	6.57×10^{12}
710	0.275	0.494	0.142	1.00	1.06×10^{14}	1.15×10^{14}
860	0.273	0.498	0.145	1.00	2.48×10^{14}	3.63×10^{14}
1050	0.272	0.496	0.145	1.00	3.53×10^{14}	7.16×10^{14}
Cumulative Abundances	0.273	0.497	0.145	1.00		
Expected Abundances	0.269	0.495	0.145	1.00		3.3×10^{15}

TABLE I-III

The Isotopic Composition and Amount of Fission Product Xenon Evolved from U_3O_8 I (Cooling Time = 20 Months) as a Function of Temperature

Temperature Plateau °C	Isotope				Xenon Atoms Released	Cumulative Xenon Atoms Released
	131	132	134	136		
140	0.387	0.538	0.918	1.092	9.7×10^{12}	9.7×10^{12}
250	1.180	0.590	0.921	1.092	1.54×10^{13}	2.51×10^{13}
380	2.750	1.093	0.965	1.092	8.53×10^{12}	3.36×10^{13}
570	1.430	1.354	1.023	1.092	1.85×10^{13}	5.33×10^{13}
710	0.450	0.619	1.002	1.092	4.33×10^{14}	4.87×10^{14}
860	0.379	0.575	0.999	1.092	1.51×10^{15}	2.00×10^{15}
1050	0.373	0.566	1.001	1.092	2.26×10^{15}	4.25×10^{15}
Cumulative Abundances	0.388	0.578	1.000	1.092		
Expected Abundances	0.364	0.544	1.000			2.0×10^{16}

The following values were used:

$$\frac{U^{235}}{U^{238}} = 0.072$$

$$\sigma_f = 590 \times 10^{-24} \text{ cm}^2$$

$$Y_{Xe} = 0.236$$

$$Y_{Kr} = 0.039$$

The cumulative amounts of krypton and xenon released were obtained by summing the amounts released up to and including each temperature plateau.

The errors of the isotope abundance data, expressed as standard deviations of seven double mass spectrometer scans varied from about 1% for the smallest samples to about 0.3% for the largest samples. The errors of the amounts of krypton and xenon released are about 5%, as determined from the errors of the mass spectrometric analyses, and the errors of the tracer determinations.

The amounts of krypton and xenon samples obtained after breaking the quartz irradiation capsule at room temperature (see Section II A 3a) were less than 0.2% of the total amounts of krypton and xenon produced.

The results for krypton (Table I-II) show that there are no significant deviations from the normal fission pattern. However, xenon exhibits marked enrichments of Xe^{131} and Xe^{132} relative to Xe^{136}, particularly for the low temperature fractions. These effects for krypton and xenon are in agreement with the results of Kennett and Thode (1960) for U_3O_8 powder.

Tables I-IV and I-V give xenon isotope abundances and amounts evolved as a function of temperature for U_3O_3 II and U_3O_8 III. Krypton results are not given since no deviations from the normal fission pattern were observed. Both powder samples were irradiated in the same self-serve position in the reactor, and for the same period of time as U_3O_8 I. Extraction of fission gas from U_3O_8 II was started 10 days after irradiation and extraction from U_3O_8 III was started 21 days after irradiation. The effect of the hold-up in the 131 chain by I^{131} ($T_{1/2}$ = 8.05 d) and in the 132 chain by Te^{132} ($T_{1/2}$ = 78 h) is seen from the depletion of the cumulative abundances of Xe^{131} and Xe^{132}, relative to the expected abundances. The isotope enrichments in Xe^{131} and Xe^{132} in low temperature fractions appear to be greater for U_3O_8 III than for either U_3O_8 I or U_3O_8 II. The significance of this will be discussed later.

Tables I-VI, I-VII and I-VIII give xenon isotope abundances and amounts evolved as a function of temperature for $UO_{2.005}$, $UO_{2.175}$ and $UO_{2.241}$ respectively. Krypton isotope abundances are not given since no deviations from the normal fission krypton pattern were observed. It may be noted that xenon evolved from $UO_{2.175}$ and $UO_{2.241}$ exhibits similar isotopic effects to xenon from U_3O_8, whereas the effects for xenon from $UO_{2.005}$, although measurable, are much smaller.

2. Diffusion Effects

For the purpose of analysis the procedure followed was to consider the diffusion system as an assembly of uniform spherical regions. The controlling parameter which approximately represents the detailed geometry of the system is then the radius of these hypothetical spheres. To obtain

TABLE I-IV

The Isotopic Composition and Amount of Fission Product Xenon Evolved from U_3O_8 II (Cooling Time = 10 Days) as a Function of Temperature

Temperature Plateau °C	Isotope 131	132	134	136	Xenon Atoms Released	Cumulative Xenon Atoms Released
125	1.042	0.713	1.102	1.112	1.71×10^{13}	1.71×10^{13}
235	3.151	1.016	1.051	1.112	9.87×10^{12}	2.70×10^{13}
380	0.678	0.676	1.003	1.112	2.36×10^{13}	5.06×10^{13}
500	0.360	0.639	1.003	1.112	5.04×10^{13}	1.01×10^{14}
700	0.270	0.560	0.997	1.112	5.80×10^{14}	6.81×10^{14}
960	0.257	0.537	1.000	1.112	1.95×10^{15}	2.63×10^{15}
1150	0.264	0.528	1.001	1.112	4.07×10^{15}	6.70×10^{15}
Cumulative Abundances	0.271	0.536	1.000	1.112		
Expected Abundances	0.364	0.544	1.000			2.3×10^{16}

TABLE I-V

The Isotopic Composition and Amount of Fission Product Xenon Evolved from U_3O_8 III (Cooling Time = 21 Days) as a Function of Temperature

Temperature Plateau °C	Isotope 131	132	134	136	Xenon Atoms Released	Cumulative Xenon Atoms Released
125	3.580	0.668	0.972	1.078	1.38×10^{13}	1.38×10^{13}
240	15.10	1.281	1.060	1.078	1.21×10^{13}	2.59×10^{13}
385	0.605	0.617	1.002	1.078	2.02×10^{13}	4.61×10^{13}
490	0.404	0.657	1.000	1.078	2.83×10^{13}	7.44×10^{13}
630	0.376	0.657	1.008	1.078	1.37×10^{13}	2.11×10^{14}
850	0.333	0.569	1.000	1.078	1.38×10^{15}	1.59×10^{15}
1100	0.332	0.553	0.998	1.078	2.99×10^{15}	4.58×10^{15}
Cumulative Abundances	0.346	0.563	1.000	1.078		
Expected Abundances	0.364	0.544	1.000			2.0×10^{16}

TABLE I-VI

The Isotopic Composition and Amount of Fission Product Xenon Evolved from $UO_{2.005}$ as a Function of Temperature

Temperature Plateau °C	Isotope				Xenon Atoms Released	Cumulative Xenon Atoms Released
	131	132	134	136		
135	0.391	0.611	0.997	1.077	1.36×10^{12}	1.36×10^{12}
250	0.404	0.626	0.988	1.077	2.97×10^{12}	4.33×10^{12}
385	0.461	0.724	0.976	1.077	1.48×10^{12}	5.81×10^{12}
540	0.436	0.641	0.956	1.077	1.16×10^{12}	7.67×10^{12}
730	0.383	0.575	1.002	1.077	1.38×10^{13}	2.14×10^{13}
840	0.379	0.563	0.998	1.077	2.22×10^{13}	4.36×10^{13}
1050	0.371	0.555	1.001	1.077	1.06×10^{14}	1.49×10^{14}
Cumulative Abundances	0.376	0.561	1.000	1.077		
Expected Abundances	0.364	0.544	1.000			2.1×10^{16}

TABLE I-VII

The Isotopic Composition and Amount of Fission Product Xenon Evolved from $UO_{2.175}$ as a Function of Temperature

Temperature Plateau °C	Isotope 131	132	134	136	Xenon Atoms Released	Cumulative Xenon Atoms Released
130	1.910	1.290	1.100	1.209	3.4×10^{11}	3.4×10^{11}
240	2.020	1.070	1.110	1.209	9.8×10^{11}	1.32×10^{12}
375	3.920	2.250	1.130	1.209	5.03×10^{11}	1.83×10^{12}
540	1.510	1.110	1.060	1.209	9.79×10^{11}	2.81×10^{12}
710	0.446	0.595	1.003	1.209	1.78×10^{13}	2.06×10^{13}
850	0.383	0.597	1.005	1.209	9.26×10^{13}	1.13×10^{14}
1015	0.370	0.565	0.997	1.209	2.28×10^{14}	3.41×10^{14}
Cumulative Abundances	0.384	0.578	1.000	1.209		
Expected Abundances	0.364	0.544	1.000			1.8×10^{16}

TABLE I-VIII

The Isotopic Composition and Amount of Fission Product Xenon Evolved from $UO_{2.241}$ as a Function of Temperature

Temperature Plateau °C	Isotope 131	132	134	136	Xenon Atoms Released	Cumulative Xenon Atoms Released
150	7.91	3.090	1.010	1.187	1.51×10^{12}	1.51×10^{12}
260	22.10	7.120	1.003	1.187	3.36×10^{12}	4.87×10^{12}
385	16.80	19.60	1.100	1.187	3.36×10^{12}	8.23×10^{12}
560	1.040	1.371	1.014	1.187	2.37×10^{13}	3.19×10^{13}
710	0.439	0.623	1.003	1.187	1.01×10^{15}	1.04×10^{15}
850	0.386	0.592	1.000	1.187	4.07×10^{15}	5.12×10^{15}
1010	0.376	0.570	0.996	1.187	2.20×10^{15}	7.31×10^{15}
Cumulative Abundances	0.393	0.592	1.000	1.187		
Expected Abundances	0.364	0.544	1.000			2.0×10^{16}

a solution, the following equation must be solved:

$$\frac{\partial c}{\partial t} = \frac{D}{r^2}\frac{\partial}{\partial r}\left(r^2 \frac{\partial c}{\partial r}\right)$$

with the following boundary conditions:

$$c = c_0 \quad \text{for} \quad t = 0$$

$$c = 0, \; r > a \quad \text{for} \quad t \geqslant 0.$$

The solution is (Barrer 1941)

$$c = -2\frac{c_0 a}{\pi r}\sum_{n=1}^{\infty}\frac{(-1)^n}{n}\exp\left(-\frac{n^2\pi^2 Dt}{a^2}\right)\sin\frac{n\pi r}{a}$$

It may readily be shown (Boyd et al 1947) that

$$f = 1 - \frac{6}{\pi^2}\sum_{n=1}^{\infty}\frac{1}{n^2}\exp\left(-\frac{n^2\pi^2 Dt}{a^2}\right)$$

where f is the fraction diffused out of the sphere in time t. The above series has been numerically evaluated by Reichenberg (1953) for values of f from 0.01 to 0.99. Booth (1957) gives the following approximation:

$$f = 6\sqrt{\frac{Dt}{\pi a^2}} \qquad \text{for } f \leqslant 0.1$$

Values of f and the diffusion parameter Dt/a^2 (for t = 3 hours in every case) for krypton and xenon and the uranium oxide systems are given in Tables I-IX to I-XIV inclusive. The values of f were obtained from the cumulative release, and the expected amounts produced by irradiation.

Plots of $\log_{10}(\frac{Dt}{a^2})$ against T^{-1} are shown in Figs. I-5 to I-8 inclusive. Activation energies, obtained from the slopes of the Dt/a^2 plots are given in Table I-XV.

TABLE I-IX

Fractional Release and the Diffusion Parameter Dt/a^2
for Krypton and Xenon from U_3O_8 I
as a Function of Temperature

Temperature Plateau °C	Krypton		Xenon	
	Fractional Release	$\frac{Dt}{a^2}$	Fractional Release	$\frac{Dt}{a^2}$
140	1.4×10^{-4}	1.7×10^{-9}	4.9×10^{-4}	2.1×10^{-8}
250	2.4×10^{-4}	5.0×10^{-9}	1.3×10^{-3}	1.4×10^{-7}
380	5.7×10^{-4}	2.8×10^{-8}	1.7×10^{-3}	2.5×10^{-7}
570	2.0×10^{-3}	3.5×10^{-7}	2.7×10^{-3}	6.2×10^{-7}
710	3.5×10^{-2}	1.1×10^{-4}	2.4×10^{-2}	5.1×10^{-8}
860	0.10	9.1×10^{-4}	0.10	9.1×10^{-4}
1050	0.22	4.7×10^{-3}	0.21	4.3×10^{-3}

TABLE I-X

Fractional Release and the Diffusion Parameter Dt/a^2
for Krypton and Xenon from U_3O_8 II
as a Function of Temperature

Temperature Plateau °C	Krypton		Xenon	
	Fractional Release	$\frac{Dt}{a^2}$	Fractional Release	$\frac{Dt}{a^2}$
125	1.2×10^{-4}	1.3×10^{-9}	7.4×10^{-4}	4.8×10^{-8}
235	2.4×10^{-4}	5.0×10^{-9}	1.2×10^{-3}	1.2×10^{-7}
380	1.4×10^{-3}	1.7×10^{-7}	2.2×10^{-3}	4.2×10^{-7}
500	4.1×10^{-3}	1.5×10^{-6}	4.4×10^{-3}	1.7×10^{-6}
700	3.1×10^{-2}	8.5×10^{-5}	3.0×10^{-2}	7.7×10^{-5}
960	7.4×10^{-2}	4.8×10^{-4}	0.11	1.1×10^{-3}
1150	0.27	7.4×10^{-3}	0.29	3.6×10^{-3}

TABLE I-XI

Fractional Release and the Diffusion Parameter Dt/a^2 for Krypton and Xenon from U_3O_8 III as a Function of Temperature

Temperature Plateau °C	Krypton		Xenon	
	Fractional Release	$\frac{Dt}{a^2}$	Fractional Release	$\frac{Dt}{a^2}$
125	1.3×10^{-4}	1.5×10^{-9}	6.9×10^{-4}	4.1×10^{-8}
240	2.2×10^{-4}	4.2×10^{-9}	1.3×10^{-3}	1.5×10^{-7}
385	1.4×10^{-3}	1.7×10^{-7}	2.3×10^{-3}	4.6×10^{-7}
490	3.1×10^{-3}	8.2×10^{-7}	3.7×10^{-3}	1.2×10^{-6}
630	1.3×10^{-2}	1.5×10^{-5}	1.1×10^{-2}	9.8×10^{-6}
850	0.11	1.1×10^{-3}	7.9×10^{-2}	5.4×10^{-4}
1100	0.23	5.2×10^{-3}	0.23	5.2×10^{-3}

TABLE I-XII

Fractional Release and the Diffusion Parameter Dt/a^2 for Krypton and Xenon from $UO_{2.005}$ as a Function of Temperature

Temperature Plateau °C	Krypton		Xenon	
	Fractional Release	$\frac{Dt}{a^2}$	Fractional Release	$\frac{Dt}{a^2}$
135	1.4×10^{-5}	1.7×10^{-11}	6.5×10^{-5}	3.7×10^{-10}
250	1.2×10^{-4}	1.3×10^{-9}	2.1×10^{-4}	3.7×10^{-9}
385	2.7×10^{-4}	6.5×10^{-9}	2.8×10^{-4}	6.7×10^{-9}
540	3.3×10^{-4}	9.4×10^{-9}	3.7×10^{-4}	1.2×10^{-8}
730	1.0×10^{-3}	8.7×10^{-8}	1.0×10^{-3}	8.7×10^{-8}
840	2.2×10^{-3}	4.1×10^{-7}	2.1×10^{-3}	3.7×10^{-7}
1085	6.8×10^{-3}	4.0×10^{-6}	7.1×10^{-3}	4.4×10^{-6}

TABLE I-XIII

Fractional Release and the Diffusion Parameter Dt/a^2 for Krypton and Xenon from $UO_{2.175}$ as a Function of Temperature

Temperature Plateau °C	Krypton		Xenon	
	Fractional Release	$\frac{Dt}{a^2}$	Fractional Release	$\frac{Dt}{a^2}$
130	3.0×10^{-6}	7.7×10^{-13}	1.9×10^{-5}	3.1×10^{-11}
240	1.4×10^{-5}	1.7×10^{-11}	7.3×10^{-5}	4.6×10^{-10}
375	3.0×10^{-5}	8.0×10^{-11}	1.0×10^{-4}	8.7×10^{-10}
540	4.1×10^{-5}	1.4×10^{-10}	1.6×10^{-4}	2.2×10^{-9}
710	1.4×10^{-3}	1.7×10^{-7}	1.1×10^{-3}	9.8×10^{-6}
850	6.9×10^{-3}	4.1×10^{-6}	6.3×10^{-3}	3.4×10^{-6}
1015	1.9×10^{-2}	3.1×10^{-5}	1.9×10^{-2}	3.1×10^{-5}

TABLE I-XIV

Fractional Release and the Diffusion Parameter Dt/a^2
for Krypton and Xenon from $UO_{2.241}$
as a Function of Temperature

Temperature Plateau °C	Krypton		Xenon	
	Fractional Release	$\frac{Dt}{a^2}$	Fractional Release	$\frac{Dt}{a^2}$
150	6.9×10^{-6}	4.1×10^{-12}	8.9×10^{-5}	6.9×10^{-10}
260	1.5×10^{-5}	1.9×10^{-11}	2.9×10^{-4}	7.2×10^{-9}
385	6.6×10^{-5}	3.8×10^{-10}	4.8×10^{-4}	2.0×10^{-8}
560	1.2×10^{-3}	1.3×10^{-7}	1.9×10^{-3}	3.1×10^{-7}
710	6.5×10^{-2}	3.7×10^{-4}	6.1×10^{-2}	3.2×10^{-4}
850	0.28	8.0×10^{-3}	0.30	9.3×10^{-3}
1010	0.40	1.8×10^{-2}	0.43	2.1×10^{-2}

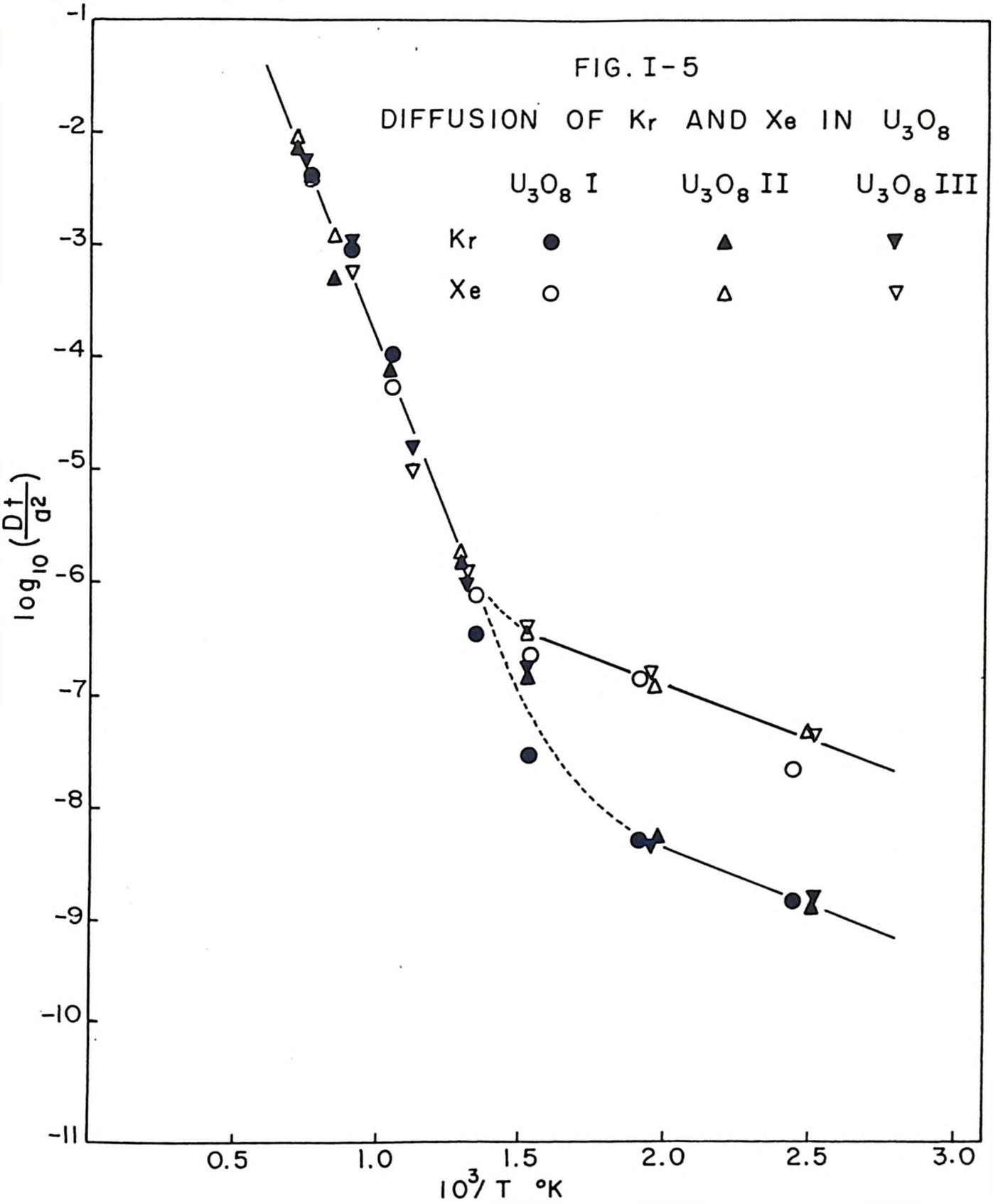
FIG. I-5
DIFFUSION OF Kr AND Xe IN U_3O_8
U_3O_8 I
U_3O_8 II
U_3O_8 III
Kr
Xe
$\log_{10}(\frac{Dt}{a^2})$
$10^3/T$ °K
-1
-2
-3
-4
-5
-6
-7
-8
-9
-10
-11
0.5
1.0
1.5
2.0
2.5
3.0

FIG. I-6

DIFFUSION OF Kr AND Xe IN $UO_{2.005}$

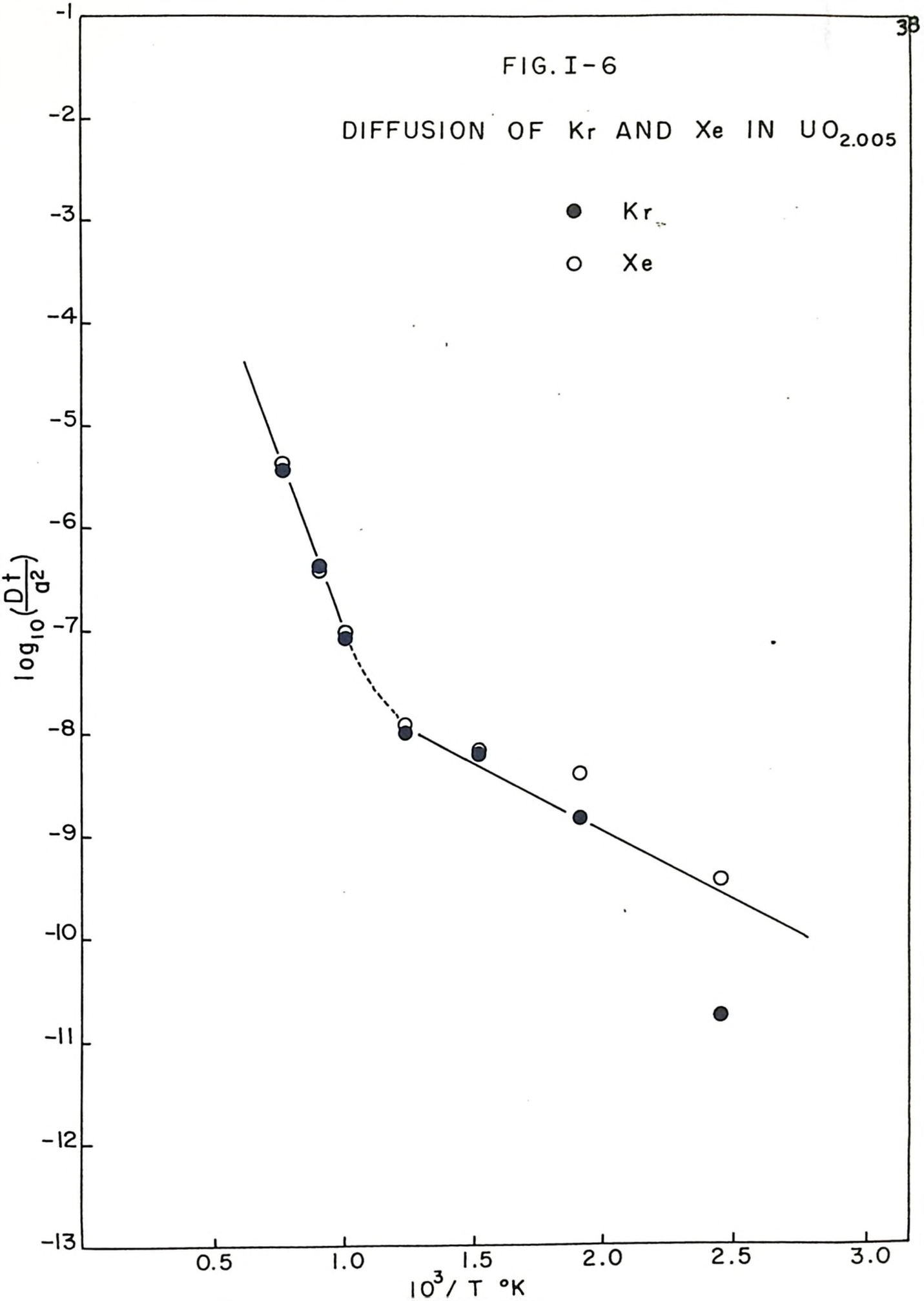

FIG. I-7

DIFFUSION OF Kr AND Xe IN $UO_{2.175}$

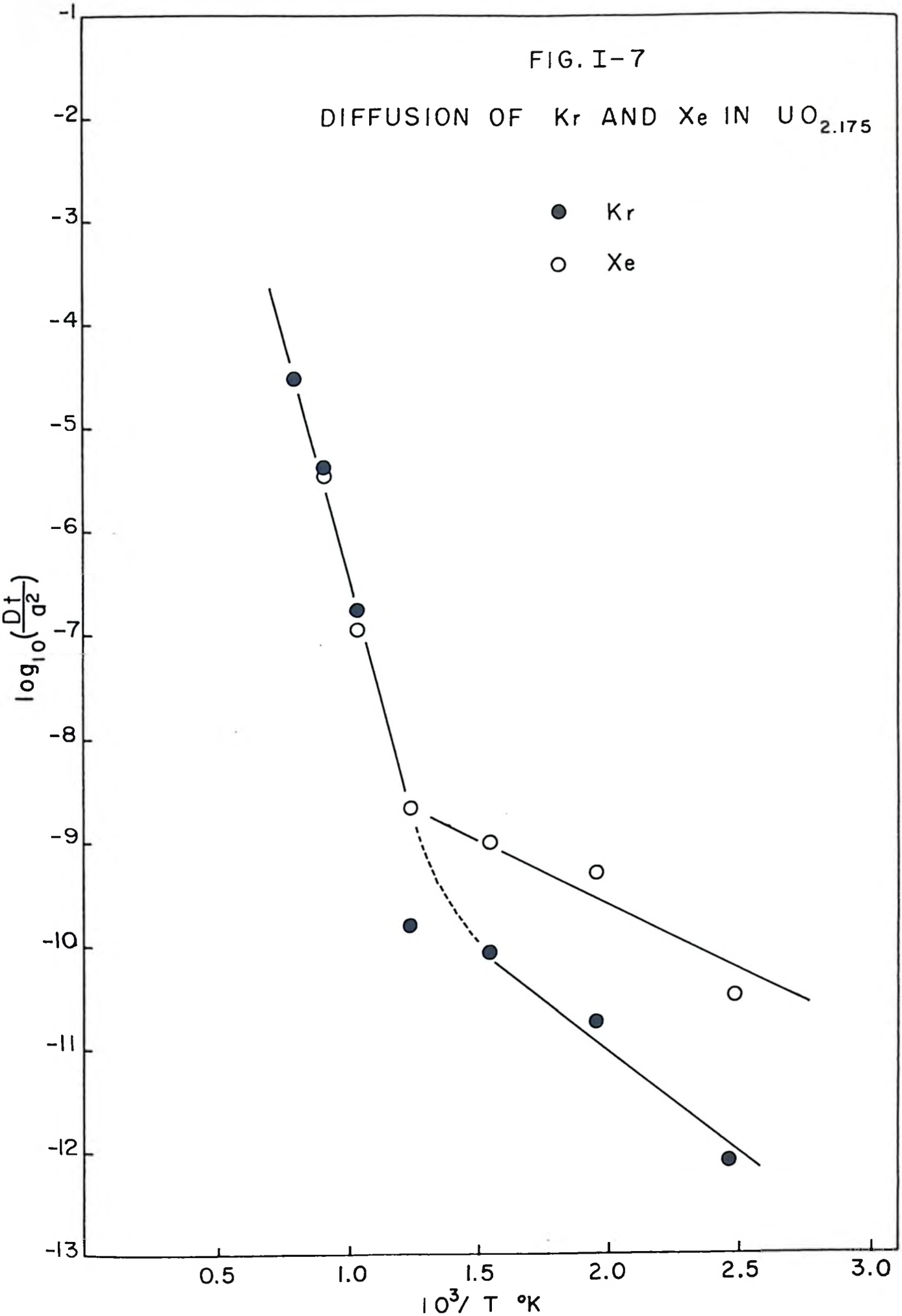

FIG. I-8

DIFFUSION OF Kr AND Xe IN $UO_{2.241}$

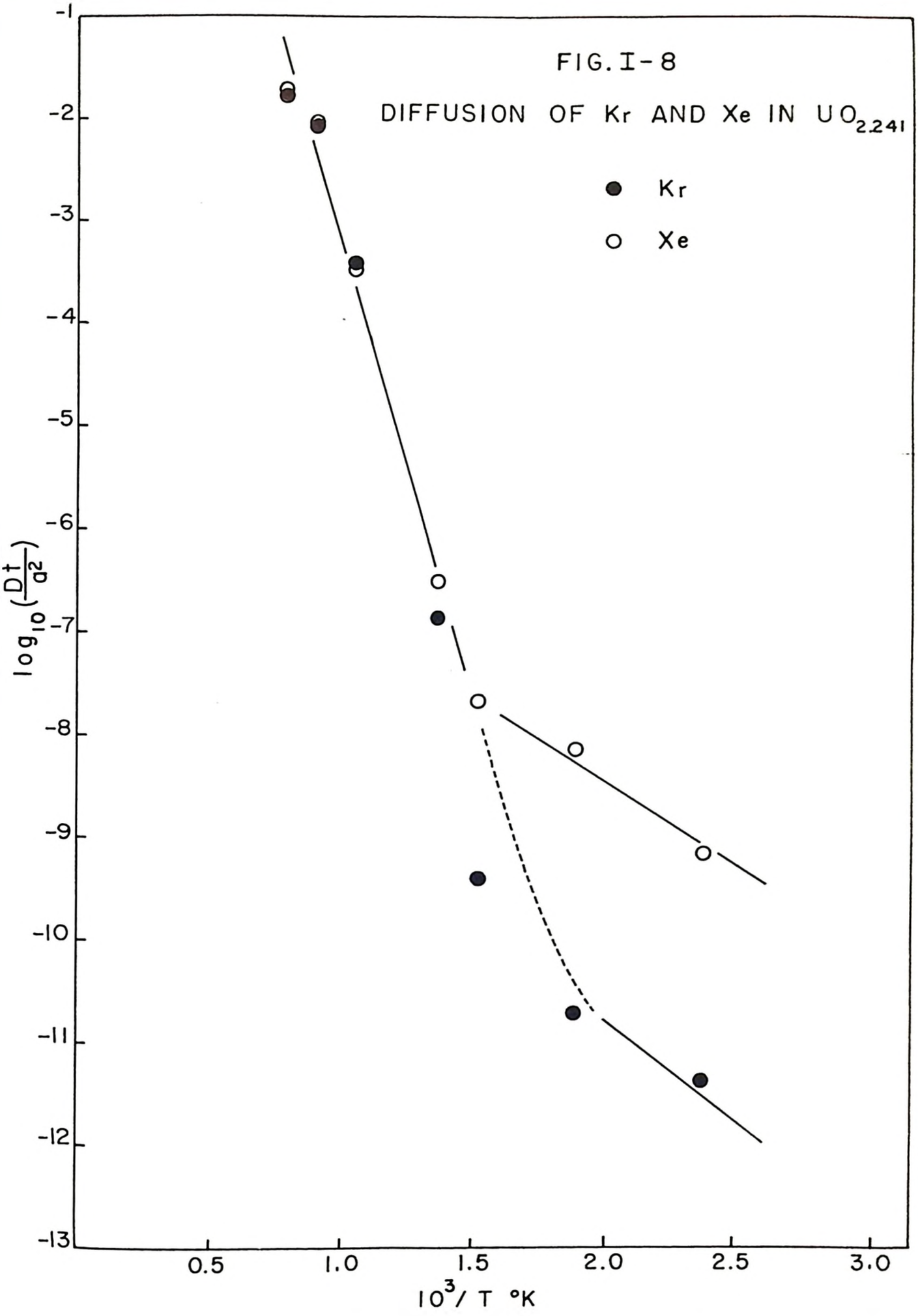

TABLE I-XV

Activation Energies in k cal/mole for Krypton and Xenon and the Uranium Oxide Systems

System	Krypton		Xenon	
	Q_1	Q_2	Q_1	Q_2
U_3O_8	27	5	27	5
$UO_{2.005}$	31	6*	31	6
$UO_{2.175}$	43	9	43	5
$UO_{2.241}$	39	10*	39	7

*Although the existence of two activation energies for the diffusion process appears certain, the Q values for krypton diffusion from $UO_{2.005}$ and $UO_{2.241}$ must be regarded as uncertain (see Figs. I-6 and I-8).

B. DIFFUSION OF STABLE KRYPTON AND XENON FROM IRRADIATED UH_3 AND UN

Samples of fission-product krypton extracted from UH_3 and UN powders over a temperature range 100°C - 1100°C did not show measurable deviations from the normal fission krypton pattern. Small enrichments of Xe^{131} and Xe^{132} (2% - 5%) were observed in low temperature fractions of fission xenon evolved from the powders. However, the effects for xenon were not considered to be significant since they could have been caused by a 0.2% - 0.5% contamination of the powders by U_3O_8. Surface oxide which would be in the form of U_3O_8 was probably not removed completely from the uranium filings used to prepare the UH_3 and UN powders.

C. DIFFUSION OF RADIOACTIVE XENON AND IODINE FROM U_3O_8

1. Xe^{133} and Xe^{135}

A one-gram sample of 200-325 mesh U_3O_8 powder was irradiated for 1 hour at a flux of about 1.4×10^{13} neutrons/cm^2/sec. After a 2-day cooling period extraction of the rare gases was started. The Xe^{133}/Xe^{135} atom ratio in each temperature fraction was determined by the relative count rates of Xe^{133} ($T_{1/2}$ = 5.27 d) and Xe^{135} ($T_{1/2}$ = 9.2 h), at the time of analysis. The Xe^{133}/Xe^{135} ratio was calculated for each temperature fraction (see Appendix A). A comparison between the experimental and calculated values is shown in Table I-XVI.

The NaI crystal was not calibrated for variation of efficiency of detection with energy. Owing to this uncertainty it is thought that the experimental values given in Table I-XVI are accurate only to about 10%.

TABLE I-XVI

Xe^{133}/Xe^{135} Ratio in Fission Gas Fractions Evolved from U_3O_8 as a Function of Temperature

Temperature Plateau °C	Xe^{133}/Xe^{135}	
	Experimental	Calculated
110	10	10
220	45	29
310	43	30
550	29	34
790	196	174
1050	128	132

2. Xe^{133} and I^{131}

A one-gram sample of 200-325 mesh U_3O_8 powder was irradiated for 1 minute at a flux of about 1.2×10^{13} neutrons/cm^2/sec. After a 10-day cooling period, extraction of Xe^{133} ($T_{1/2}$ = 5.27 d) and I^{131} ($T_{1/2}$ = 8.05 d) was started.

The results of the analysis by scintillation counting are shown in Table I-XVII. The duration of analysis of the samples was about 1 hour, so no correction for decay of I^{131} or Xe^{133} during analysis was necessary.

The I^{131}/Xe^{133} atom ratio at the time of analysis was calculated in a similar manner to the Xe^{133}/Xe^{135} calculation, and was found to be 2.7. Since 81% of the I^{131} decays are via the 364-kev γ-ray and 100% of the Xe^{133} decays are via the 81-kev γ-ray, the value for I^{131}/Xe^{133} (970°C) found experimentally is

$$\frac{2.2}{1.7} \times \frac{100}{81} \times \frac{8.05}{5.27} = 2.4$$

which is in fair agreement with the calculated value of 2.7. Hence it was assumed that the fractional cumulative release of I^{131} was equal to that of Xe^{133} at 970°C. It was also assumed that the fractional cumulative release of Xe^{133} at 970°C was equal to the fractional cumulative release of stable xenon isotopes at the same temperature from U_3O_8 powder of the same particle size, i.e. about 0.12 (see Table I-X).

Values of f (fractional cumulative release) and the diffusion parameter Dt/a^2 as a function of temperature, for I^{131} and Xe^{133} are given in Table I-XVIII.

TABLE I-XVII

Cumulative Count Rate of I^{131} and Xe^{133} Evolved from U_3O_8 as a Function of Temperature

Temperature Plateau °C	Cumulative Counts/Minute	
	I^{131} (364 Kev)	Xe^{133} (81 Kev)
115	2.6×10^3	3.8×10^2
235	5.2×10^3	1.3×10^3
380	9.6×10^3	3.7×10^3
610	2.1×10^4	1.5×10^4
970	2.2×10^5	1.7×10^5

TABLE I-XVIII

Values of f and Dt/a^2 for I^{131} and Xe^{133} Evolved From U_3O_8 as a Function of Temperature

Temperature Plateau °C	I^{131}		Xe^{133}	
	f	Dt/a^2	f	Dt/a^2
115	1.4×10^{-3}	1.7×10^{-7}	2.7×10^{-4}	6.3×10^{-9}
235	2.8×10^{-3}	6.8×10^{-7}	9.2×10^{-4}	7.4×10^{-8}
380	5.2×10^{-3}	2.4×10^{-6}	2.6×10^{-3}	5.9×10^{-7}
610	1.5×10^{-2}	1.9×10^{-5}	1.1×10^{-2}	1.1×10^{-5}
970	0.12	1.3×10^{-3}	0.12	1.3×10^{-3}

A plot of $\log_{10}(\frac{Dt}{a^2})$ against T^{-1} for I^{131} and Xe^{133} in the U_3O_8 system is shown in Fig. I-9. From the slopes of the Dt/a^2 plot the following activation energies were calculated:

I^{131} - 28 k cal/mole, 5 k cal/mole.

Xe^{133} - 28 k cal/mole, 7 k cal/mole.

The activation energies for Xe^{133} are in fair agreement with the activation energies for diffusion of stable xenon from U_3O_8 (see Table I-XV).

FIG. I-9

DIFFUSION OF I^{131} AND Xe^{133} IN U_3O_8

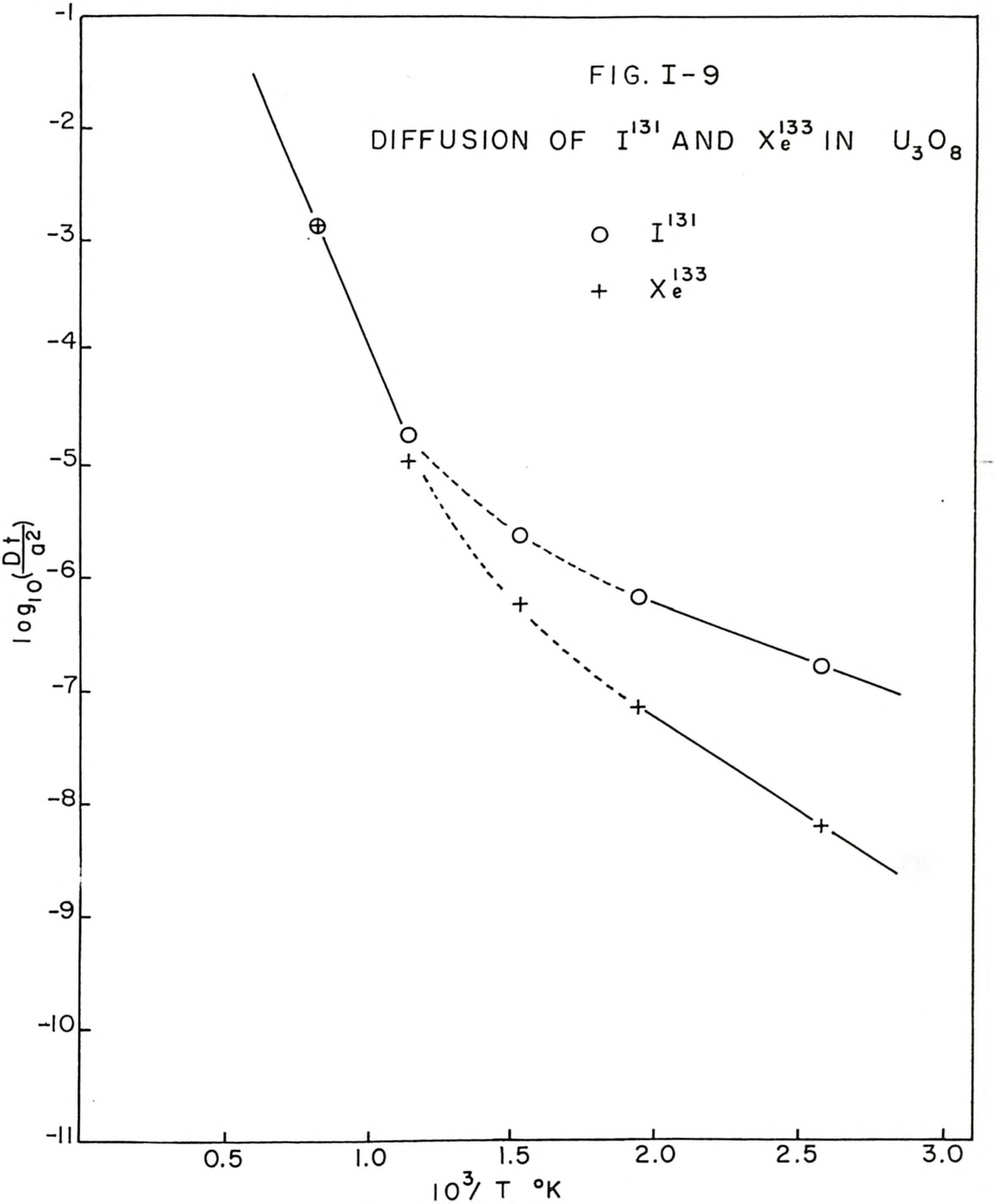

IV. DISCUSSION

A. THE Xe^{131}, Xe^{132} AND Xe^{134} ANOMALIES

1. Qualitative Description

It is apparent that for fission-product xenon released at low temperatures (< 600°C) from irradiated uranium oxides, the abundances of Xe^{131} and Xe^{132} (relative to the abundance of Xe^{136}) are far higher than would be expected from known data on xenon fission yields in the thermal neutron fission of U^{235}.

Kennett and Thode (1960) suggested that the isotope effects observed by them for Xe^{131} and Xe^{132} released from U_3O_8 at low temperatures were correlated in some way with the decay characteristics of the precursors of xenon (i.e. iodine, tellurium, etc.) and that the diffusion properties of the precursors in the U_3O_8 system are quite different from the diffusion properties of xenon in the U_3O_8 system at low temperatures. In a qualitative way, an explanation of the isotope effects could be given by the following description:

Diffusion of precursors of xenon is more rapid than diffusion of xenon to the surface of particles or to grain boundaries either during or after irradiation. Precursors having long half-lives for decay will be concentrated to a greater extent on the surface of particles or in grain boundaries than precursors having short half-lives. Subsequent decay of precursors to stable xenon isotopes will cause an enrichment of the isotopes of xenon having long-lived precursors relative to isotopes of

xenon having short-lived precursors. During subsequent heating experiments, xenon on particle surfaces or in grain boundaries will be released more rapidly at low temperatures than xenon trapped in the uranium oxide lattice. The isotopic composition of xenon released at low temperatures will thus be different from the isotopic composition of the total xenon in the system.

The fission-product decay chains for masses 131, 132, 134 and 136 are shown in Table I-XIX. It is seen that the half-lives of precursors mainly responsible for hold-up in the fission chains decrease markedly from the 131 chain to the 136 chain.

2. Theory

For the purpose of analysis, let us consider the following decay chain

$$X_1 \xrightarrow{\lambda_1} X_{2(\text{stable})}$$

If we consider a sphere model for the powder-fission-product diffusion system, then to obtain a solution to the problem the following equations must be solved (with the appropriate boundary conditions):

$$\frac{\partial c_1}{\partial t} = \frac{D_1}{r^2}\frac{\partial}{\partial r}\left(r^2\frac{\partial c_1}{\partial r}\right) - \lambda_1 c_1 + B_1 \qquad (1)$$

$$\frac{\partial c_2}{\partial t} = \frac{D_2}{r^2}\frac{\partial}{\partial r}\left(r^2\frac{\partial c_2}{\partial r}\right) + \lambda_1 c_1 + B_2 \qquad (2)$$

$$\frac{\partial c_1}{\partial t} = \frac{D_1'}{r^2}\frac{\partial}{\partial r}\left(r^2\frac{\partial c_1}{\partial r}\right) - \lambda_1 c_1 \qquad (3)$$

$$\frac{\partial c_2}{\partial t} = \frac{D_2'}{r^2}\frac{\partial}{\partial r}\left(r^2\frac{\partial c_2}{\partial r}\right) + \lambda_1 c_1 \qquad (4)$$

TABLE I-XIX

Fission-Product Decay Chains for Masses
131, 132, 134 and 136

Mass	Nuclear Charge					Chain Yield %
	50	51	52	53	54	
131	Sn (3.4 m)	→ Sb (22 m)	→ Te (25 m)	→ I (8.05 d)	→ Xe	2.9
		15% → Te (30 h)				
		85% → Te (25 m)				
132	Sn (2.2 m)	→ Sb (1.9 m)	→ Te (77.7 h)	→ I (2.33 h)	→ Xe	4.3
134		Sb (45 s)	→ Te (44 m)	→ I (52.5 m)	→ Xe	7.9
136			Te (20 s)	→ I (86 s)	→ Xe	6.4

Note: Numbers in brackets are decay half-lives.

Equations (1) and (2) describe the diffusion system during irradiation; equations (3) and (4) describe the diffusion system after irradiation. B_1 and B_2 are constant production rates of X_1 and X_2 during irradiation. D_1 and D_2 are diffusion coefficients of X_1 and X_2 during irradiation; D_1' and D_2' are diffusion coefficients of X_1 and X_2 after irradiation. c_1 and c_2 are concentrations of X_1 and X_2 as a function of r and time, where r is the distance from the centre of the hypothetical sphere (of radius a).

Let us first consider the system after irradiation, and make the following simplifying assumptions:

1) $D_1' \gg D_2'$

2) $B_2 \ll B_1$

Assumption 2) is valid for the 131, 132, 134 and 136 chains since the primary yield of stable xenon is much smaller than the primary yield of either iodine or tellurium for a particular decay chain. The validity of assumption 1) will be discussed later.

Hence, we require a solution to equation (3) with the following boundary conditions:

$$c_1 = c_0 \text{ for } t = 0$$

$$c_1 = 0, \; r > a \text{ for } t \geqslant 0.$$

The solution to equation (3) is analagous to the solution given for the case $\lambda_1 = 0$ (see Section II A 2) and is

$$c_1 = -\frac{2c_0 a}{\pi r} \sum_{n=1}^{\infty} \frac{(-1)^n}{n} \exp\left(\frac{-n^2\pi^2 D_1' t}{a^2}\right) \exp(-\lambda_1 t) \sin\frac{n\pi r}{a}$$

It may readily be shown that

$$\bar{c}_1 = -\frac{6c_0}{\pi^2} \sum_{n=1}^{\infty} \frac{1}{n^2} \exp\left(\frac{-n^2\pi^2 D_1' t}{a^2}\right) \exp(-\lambda_1 t)$$

where $\bar{c}_1$ is the average concentration of X_1 inside the hypothetical sphere at time t.

A further approximation is now made by assuming that escape of X_1 from the sphere is a small fraction (< 0.1) of the initial amount $\frac{4}{3}\pi a^3 c_0$. Hence the approximation given by Booth (1957) can be used, and $\bar{c}_1$ is given by

$$\bar{c}_1 = c_0\left(1 - 6\sqrt{\frac{D_1' t}{\pi a^2}}\right) \exp(-\lambda_1 t).$$

During a cooling time t, the amount of X_2 formed from decay of X_1 is given by

$$N_2 = \tfrac{4}{3}\pi a^3 c_0 (1 - \exp(-\lambda_1 t))$$

And the amount of X_2 formed inside the hypothetical sphere is given by

$$N_2^* = \tfrac{4}{3}\pi a^3 \lambda_1 \int_0^t \bar{c}_1 \, dt$$

$$= \tfrac{4}{3}\pi a^3 \left[c_0(1 - \exp(-\lambda_1 t)) - 6\lambda_1 c_0 \sqrt{\frac{D_1'}{\pi a^2}} \int_0^t t^{1/2} \exp(-\lambda_1 t) dt\right]$$

Hence the amount of X_1 plus X_2 present outside the sphere after time t is given by

$$n_{12} = \frac{4}{3}\pi a^3 \left[6c_0 \sqrt{\frac{D_1' t}{\pi a^2}} \exp(-\lambda_1 t) + 6\lambda_1 c_0 \sqrt{\frac{D_1'}{\pi a^2}} \int_0^t t^{1/2} \exp(-\lambda_1 t)dt \right]$$

$$= 8a^2 c_0 \sqrt{D_1' \pi} \left[\sqrt{t} \exp(-\lambda_1 t) + \lambda_1 \int_0^t t^{1/2} \exp(-\lambda_1 t)dt \right] \quad (5)$$

If $t \to \infty$ (cooling time long compared with half-life of X_1), then the above expression reduces to

$$n_{12} = 8\, a^2 c_0 \sqrt{D_1' \pi}\ \lambda_1 \int_0^\infty t^{1/2} \exp(-\lambda_1 t)dt$$

$$= K \frac{c_0}{\sqrt{\lambda_1}} \quad \text{where } K = 4\, a^2 \pi \sqrt{D_1'}$$

Values of D_1' will differ slightly for isotopes of the same element, since D_1' is proportional to $(M)^{-1/2}$ (for a constant temperature) where M is the mass number. However, negligible error is introduced if D_1', and hence K, is assumed constant for isotopes of the same element. Hence the quantity $\frac{c_0}{\sqrt{\lambda_1}}$ for a particular decay chain is proportional to the isotope abundance of the stable xenon member of the chain formed from the decay of precursor which escaped from the hypothetical sphere (i.e. xenon on particle surfaces or in grain boundaries).

In the simplest case, it is assumed that $D'(I) \gg D'(Te)$, i.e. there is negligible concentration of tellurium on particle surfaces or in grain boundaries as compared to iodine. In this case c_0 for a particular decay chain is the concentration of iodine at the end of irradiation and λ_1 is the effective decay constant of the isotope of iodine being considered.

In the next case, it is assumed that $D'(I) = D'(Te)$. The calculations for the 131 chain are unchanged, since I^{131} is responsible for the major hold-up in the 131 chain. For the 132 chain, since $c_0(Te) \gg c_0(I)$ for an irradiation time of 100 hours, only Te^{132} need be considered. For the 134 chain, c_0 is the sum of the concentrations of Te^{134} and I^{134} at the end of irradiation. A half-life of 1.2 hours is assumed for the decay of Te^{134} plus I^{134}.

Two of the oxide samples ($UO_{2.175}$ and $UO_{2.241}$) were irradiated continuously for 100 hours, whereas the other four (U_3O_8 I, U_3O_8 II, U_3O_8 III and $UO_{2.005}$) were irradiated when the reactor was not operated continously. It was assumed that concentration of precursors on particle surfaces or in grain boundaries takes place mainly during the cooling period after irradiation. Although the validity of this assumption will be discussed later (see Section 3b), it may be noted at this stage that heating of the powder sample during irradiation, due to conversion of kinetic energy of fission fragments into heat, could cause most of the precursors and xenon formed from decay of the precursors on particle surfaces or in grain boundaries to escape into the gas phase, i.e. the vacuum in the quartz irradiation capsule. Hence for oxide samples, which were irradiated either continuously or intermittently, it is assumed that concentration of precursors on particle surfaces or in grain boundaries effectively begins only after the oxide sample has been removed from the reactor core. The results of the calculations of $\frac{c_0}{\sqrt{\lambda_1}}$ for the two assumptions of relative diffusion rates of iodine and tellurium, and the two types of irradiation history are given in Table I-XX. The values of $\frac{c_0}{\sqrt{\lambda_1}}$

TABLE I-XX

Values of $c_0/\sqrt{\lambda_1}$ for the 131, 132 and 134 Chains

Assumption	Continuous Irradiation			Intermittent Irradiation		
	131	132	134	131	132	134
$D'(I) \gg D'(Te)$	1.00	0.045	0.004	1.00	0.061	0.006
$D'(I) = D'(Te)$	1.00	0.73	0.009	1.00	1.21	0.010

are normalised to $\frac{c_0}{\sqrt{\lambda_1}}(131) = 1.00$ for comparison. Values of $\frac{c_0}{\sqrt{\lambda_1}}(136)$ are not given since they are negligible as compared to $\frac{c_0}{\sqrt{\lambda_1}}$ values for the other three mass chains, owing to the short half-life of I^{136}. In the following discussion it will be assumed that all values of $\frac{c_0}{\sqrt{\lambda_1}}(136)$ are zero.

3. Comparison of Theory with Experiment

a. Isotope Anomalies in Xenon Evolved from U_3O_8 I, $UO_{2.175}$ and $UO_{2.241}$

For fractions of xenon collected during each 3-hour constant-temperature heating period, the isotopic composition of the "anomalous" component is expressed in the following way:

$$\Delta_i = \left(\frac{Xe^i}{Xe^{136}}\right)_{T^oC} - \left(\frac{Xe^i}{Xe^{136}}\right)_E$$

where i = 131, 132, 134 and $(Xe^i/Xe^{136})_E$ is the ratio expected from known data on xenon yields in thermal neutron fission of U^{235}.

The Δ_i values are assumed to represent the isotope abundances of xenon on particle surfaces or in grain boundaries, released during each 3-hour constant-temperature heating period. This assumption is only approximate, but should be good provided the isotope anomalies are large.

Tables I-XXI, I-XXII and I-XXIII give Δ_i values (normalised to $\Delta_{131} = 1.00$) for xenon evolved at low temperatures ($< 600^oC$) from U_3O_8 I, $UO_{2.175}$ and $UO_{2.241}$. Cumulative values of Δ_i are given in the last row of each Table and these values represent the isotopic composition of the total anomalous xenon evolved at temperatures below 600°C. Since cooling times were long for these samples, the Δ_i values may be compared with values of $\frac{c_0}{\sqrt{\lambda_1}}$ given in Table I-XX. From this comparison it appears that the assumption D'(I) = D'(Te) gives closer agreement between theory and experiment than the assumption $D'(I) \gg D'(Te)$.

From Tables I-XXI, I-XXII and I-XXIII it is also seen that the isotopic composition of anomalous xenon does not remain constant with temperature. Although the scatter in Δ_{134} values could be due to mass spectrometric error, the scatter in Δ_{132} values could not be due to mass spectrometric error. A possible explanation has been given by Lewis (1960) who suggests that β or γ decay of precursors of xenon adhering to particle surfaces may drive the daughter product by recoil back into the solid. Since decay energies are different for different precursors, the xenon isotopes formed in this way would be retained in slightly different environments in the system and hence might be released at different rates during subsequent heating experiments.

b. Isotope Anomalies in Xenon Evolved from U_3O_8 I, U_3O_8 II and U_3O_8 III

It is seen from Tables I-III, I-IV and I-V that the xenon isotope anomalies observed for low temperature fractions of xenon evolved from U_3O_8 III (cooling time = 20 days) are larger than isotope anomalies observed for either U_3O_8 II (cooling time = 10 days) or U_3O_8 I (cooling time = 20 months). This may be interpreted by assuming that concentration of precursors on particle surfaces or in grain boundaries takes place mainly after the irradiation period, and that during the cooling period back diffusion of anomalous xenon into the solid and/or diffusion of xenon in the lattice to particle surfaces or grain boundaries tends to gradually decrease the isotope enrichments.

c. Isotope Anomalies in Xenon Evolved from $UO_{2.005}$

Isotope anomalies for xenon evolved from $UO_{2.005}$ were much smaller than the anomalies observed for the other uranium oxides studied in this work. Three possible explanations could be given.

TABLE I-XXI

Isotopic Composition of Anomalous Xenon Evolved from U_3O_8 I as a Function of Temperature

Temperature Plateau °C	Isotope 131	132	134
250	+ 1.000	+ 0.056	- 0.097
380	+ 1.000	+ 0.230	- 0.015
570	+ 1.000	+ 0.760	+ 0.026
Cumulative	+ 1.000	+ 0.512	- 0.03

TABLE I-XXII

Isotopic Composition of Anomalous Xenon Evolved from $UO_{2.175}$ as a Function of Temperature

Temperature Plateau °C	Isotope 131	132	134
130	+ 1.000	+ 0.481	+ 0.064
240	+ 1.000	+ 0.317	+ 0.066
375	+ 1.000	+ 0.480	+ 0.037
540	+ 1.000	+ 0.496	+ 0.052
Cumulative	+ 1.000	+ 0.426	+ 0.051

TABLE I-XXIII

Isotopic Composition of Anomalous Xenon Evolved from $UO_{2.241}$ as a Function of Temperature

Temperature Plateau °C	Isotope 131	132	134
150	+ 1.000	+ 0.338	+ 0.001
260	+ 1.000	+ 0.303	+ 0.0001
385	+ 1.000	+ 1.158	+ 0.061
560	+ 1.000	+ 1.223	+ 0.021
Cumulative	+ 1.000	+ 0.852	+ 0.010

1. That concentration of precursors on particle surfaces, or in grain boundaries, is less effective than concentration of xenon.

2. That grain boundaries are not present to the same degree in the $UO_{2.005}$ system as compared to the other oxide systems.

3. That back diffusion of anomalous xenon is more rapid in the $UO_{2.005}$ system than in the other oxide systems.

B. THE Xe^{133}/Xe^{135} ANOMALY

It is apparent that the Xe^{133}/Xe^{135} ratio is not constant for fission gas fractions evolved at low temperatures (220°C, 310°C) from irradiated U_3O_8 (see Table I-XVI). The Xe^{133}/Xe^{135} ratio found for the above two temperatures is about a factor of 1.5 greater than the Xe^{133}/Xe^{135} ratio calculated as shown in Appendix A. If it is assumed that this discrepancy is due to rapid diffusion of precursors of xenon to particle surfaces or grain boundaries, a value for the discrepancy can be calculated in a similar manner to the method outlined in Section 2. The following assumptions are made:

1. Only I^{133} ($T_{1/2}$ = 20.8 h) and I^{135} ($T_{1/2}$ = 6.7 h) need be considered as precursors of Xe^{133} and Xe^{135}.

2. That there is negligible depletion of Xe^{135} during irradiation due to neutron capture.

The ratio of $\frac{c_0}{\sqrt{\lambda_1}}$ values for the 133 and 135 chains is found to be 1.3, which is in fair agreement with the experimental factor of 1.5.

C. THE I^{131} - Xe^{133} EXPERIMENT

This experiment illustrates the difference between the diffusion properties of iodine and xenon at low temperatures. At low temperatures (< 500°C), for the extraction from U_3O_8, the fractional release of I^{131}

is several times greater than the fractional release of Xe^{133}. This may be interpreted by assuming that I^{131} ($T_{1/2}$ = 8.05 d) has a greater tendency to concentrate at grain boundaries than I^{133} ($T_{1/2}$ = 20.8 h) and that any isotope of iodine has a greater tendency to concentrate at grain boundaries than any isotope of xenon in the U_3O_8 system. The results of this experiment therefore add support to two assumptions made during the discussion in Section 2, viz. 1) an isotope of iodine with a long half-life will be concentrated at grain boundaries to a greater extent than an isotope of iodine with a short half-life and 2) $D'(I) \gg D'(Xe)$ for the U_3O_8 system.

D. THE ABSENCE OF ISOTOPE ANOMALIES FOR KRYPTON

The absence of measurable isotope anomalies for krypton can be explained by the following:

1. Half-lives of precursors of krypton are much shorter than half-lives of xenon precursors. Br^{83} ($T_{1/2}$ = 2.33 h) is the longest-lived of the precursors of krypton formed to an appreciable extent in fission.

2. $D'(Br\ etc.) \gg D'(Kr)$ may not be valid.

3. Back diffusion of anomalous krypton may be much more rapid than back diffusion of anomalous xenon.

E. SUMMARY

1. The results of Kennett and Thode (1960) for fission-product rare gas diffusion from U_3O_8 have been confirmed.

2. Isotope enrichments in Xe^{131} and Xe^{132} are also found for low temperature fractions of fission-product xenon from other uranium oxides.

3. A simple sphere model for diffusion and decay of the xenon precursors (iodine and tellurium) accounts reasonably well for the results obtained. The above model predicts that precursors of long half-life will be concentrated in grain boundaries or on particle surfaces (regions of low activation energy) to a greater degree than precursors with short half-life.

4. The results of the Xe^{133} - Xe^{135} experiment add support to the above prediction.

5. Direct experimental evidence of the concentration of fission-product iodine in regions of low activation energy also adds support to the mechanism of concentration of precursors in regions of low activation energy.

PART II

ISOTOPE EFFECTS IN FISSION-PRODUCT RARE GASES IN THE ATMOSPHERE AND IN NATURAL GAS

I. INTRODUCTION

A. XENON AND KRYPTON ISOTOPE PATTERNS: THE ATMOSPHERE VERSUS METEORITES

The atmosphere is known to contain krypton ($\sim$ 1 part in 10^6) and xenon ($\sim$ 1 part in 2×10^7). Several authors have speculated as to whether part of the krypton and xenon in the atmosphere is of fission origin. Khlopin, Gerling and Baranovskaya (1947) reported a xenon-argon ratio of 0.02 in a uraninite from Cheraya Salma in the Karelo-Finnish S.S.R. as against a ratio of 0.00001 in the atmosphere. They attributed the high ratio to the presence of fission-product xenon in the mineral. Khlopin and Gerling (1948) calculated that during the last 2×10^9 years, the spontaneous fission of U^{238} contained in the earth's crust had produced about 0.5% of the total quantity of xenon in the atmosphere.

The first determination of the isotopic composition of fission product krypton and xenon in pitchblende was obtained by Macnamara and Thode (1950). These authors demonstrated that the krypton and xenon in the pitchblende was of different isotopic composition to atmospheric krypton and xenon, and the rare gases in the mineral were therefore of radiogenic origin as Khlopin et al had suggested.

Festa and Santangelo (1952) made a calculation similar to that of Khlopin and Gerling and found that spontaneous fission of U^{238} in the last 3.3×10^9 years in the different geospheres had produced only about 0.004% and 0.3% of the present total of atmospheric krypton and xenon respectively, and thus concluded that fission was an unimportant source of krypton and xenon in the earth's atmosphere.

Recently, Reynolds (1960a) discovered that the isotopic composition of xenon in the Richardton stone meteorite was different to the isotopic composition of xenon in the atmosphere. The most striking feature was a large excess of Xe^{129} in Richardton xenon as compared to the abundance of Xe^{129} in the atmosphere. Reynolds attributed this excess, as had been earlier proposed by Brown (1947), to decay of I^{129} ($T_{1/2} = 1.7 \times 10^7$ y). Since it has been established, by a variety of dating methods, that the solar system formed about 4.8×10^9 years ago, I^{129} is not present now, but must have been present in the early history of the solar system, and was incorporated into the meteorite parent bodies at the time of their formation. Reynolds also found curious anomalies in the abundances of the other isotopes of xenon in Richardton as compared to the abundances of these isotopes in the atmosphere.

Kuroda (1960) treated this problem on a quantitative basis and showed that if the meteoritic xenon and atmospheric xenon isotope patterns were normalised to the "shielded" isotope Xe^{130}, there appeared to be a definite excess of the isotopes Xe^{131}, Xe^{132}, Xe^{134} and Xe^{136} in the atmosphere. For example, the Xe^{136}/Xe^{130} ratio in the atmosphere is 10% greater than the Xe^{136}/Xe^{130} ratio in Richardton. Since the isotopes $Xe^{131-136}$ are the isotopes of xenon produced chiefly in fission, it was natural for Kuroda to propose that atmospheric xenon contained a portion of fission-product gas.

Kuroda carried out a calculation similar to that of Khlopin et al (1948) and showed that only about 1% of the excess Xe^{136} in the atmosphere could have arisen from spontaneous fission of U^{238}. He suggested that spontaneous fission of an extinct transuranium element such as Pu^{244},

which has an α-decay half-life of 7.6×10^7 years, and a spontaneous fission half-life of 2.5×10^{10} years, could have been responsible for the inventory of fission-product xenon in the atmosphere. Unfortunately there has as yet been no determination of the fission-product mass-yield curve for the spontaneous fission of Pu^{244}. Kuroda expressed concern with the Pu^{244} interpretation of the atmospheric excess of the heavy xenon isotopes; he noted that the excess in Xe^{132} was considerably greater than Xe^{131}, Xe^{134} or Xe^{136}, and attributed this tentatively to fine structure in the mass-yield curve of Pu^{244}. An alternative explanation will be given later in this thesis.

Since Reynolds reported the existence of differences between Richardton xenon and atmospheric xenon, it has been firmly established that xenon in many other stone meteorites is enriched in Xe^{129} from radioactive decay of extinct I^{129} (Reynolds 1960b, 1960c, 1960d; Signer 1960; Zähringer and Gentner 1961; Clarke and Thode 1961). The anomalies in the other isotopes of xenon found by Reynolds have been confirmed by the last-named authors above. Although Kuroda did not consider the abundances of the isotopes of xenon not formed by beta decay of fission products - the "shielded" isotopes Xe^{124}, Xe^{126} and Xe^{123}, it appears nonetheless that there is a definite meteoritic excess of these isotopes, which may be due to spallation reactions in the early history of the solar nebula, as proposed by Goles and Anders (1961).

This thesis is mainly concerned with the "fission" anomalies, although the Xe^{129} anomaly and the "shielded" anomalies were observed and are discussed briefly. The purpose of this work was to determine the isotopic composition of xenon in some stone meteorites and to examine in

particular the differences in the abundances of the isotopes $Xe^{131-136}$ in the light of Kuroda's hypothesis. Since krypton is also produced in fission, analyses of meteoritic krypton and atmospheric krypton were undertaken in order to search for similar isotope effects.

B. XENON AND KRYPTON ISOTOPE PATTERNS: NATURAL GAS VERSUS THE ATMOSPHERE

The rare gases helium, argon and radon occur in certain oil and gas fields in the United States and Canada. The origin of helium, argon and radon in these natural gases has been the subject of considerable speculation. The He^4 in natural gases is presumably the product of radioactive decay of U^{238}, U^{235} and Th^{232} and their daughter products. Although no direct correlation has been found between the amounts of helium and radon in natural gases (Faul et al 1954; Sakakura et al 1959), Wasserburg et al (1957) have shown that the ratio of radiogenic helium to radiogenic argon was about 10 for four helium wells in the Texas Panhandle. This ratio is approximately equal to that expected from the present-day production rates of He^4 and A^{40} in rocks containing "normal" amounts of uranium, thorium and potassium (3 ppm U, 10ppm Th and 3% K). In a more recent study, Zartman et al (1961) have investigated 39 samples of natural gas having widely different chemical compositions and geological occurrences. The ratio of radiogenic helium to radiogenic argon was shown to vary from 1.6 to 130, with most samples having values between 6 and 25. They concluded that the natural gases have been derived from rather normal rock types and in no way could the radiogenic contents have been derived from a rock reservoir greatly enriched in uranium and/or thorium.

In a preliminary study in this laboratory, Young et al (1957) examined the isotopic composition of krypton and xenon in two natural gases containing about 1% helium. They found no certain differences in the isotopic composition of krypton and xenon from natural gas as compared to the isotopic composition of krypton and xenon in the atmosphere. This indicated only a negligible contribution of fission-product krypton or xenon in natural gas. However, the samples of rare gas were small and consequently the precision of isotope abundance measurements was only about 2%. During this work the precision of isotope abundance measurements on small rare gas samples was improved considerably by use of the static method of analysis (see Part I, Section II, B 2b) and it was reasoned that a further search for krypton and xenon of fission origin in various natural gas samples might prove fruitful.

The isotopic analyses of rare gases in natural gas were undertaken with the following objectives in mind:

1. To determine whether there was a contribution of fission-product krypton or xenon in natural gas.

2. To determine whether the fission-product component (if any) in xenon was of "normal" isotopic composition, or contained an excess of Xe^{131} and Xe^{132}, which could be explained by analogy with the results reported in Part I of this thesis.

II. EXPERIMENTAL

A. EXTRACTION OF RARE GASES FROM STONE METEORITES

1. The Vacuum Induction Furnace

The meteorite samples were heated in the vacuum induction furnace shown in Fig. II-1. Samples were placed in the molybdenum crucible E, which was placed in two concentric "Lava" (an artificial ceramic) holders D and B. A molybdenum radiation shield C placed around the outer "Lava" holder reduced radiation losses. The crucible absorbed radiofrequency power from the tank coil F. A six-kilowatt Ajax Northrup mercury-arc converter supplied power to the coil. The device used to cycle the power on and off and thus control the temperature attained by the crucible has been described in detail by Young (1953).

2. Extraction and Purification of Rare Gases

The crucible was charged with 10 - 30 gms of stone meteorite, either in the form of chips broken off from the main specimen, or as powder which had passed through an 80-mesh screen. The "Lava" assembly, containing the crucible, was lowered into the quartz envelope, the pyrex tube A was then sealed, and the furnace compartment pumped out through a large bore mercury valve G shown in Fig. II-2. During a 12-hour pumping period the titanium furnaces were held at about 800°C and the charcoal trap and sample tubes S_1 and S_2 heated to about 300°C. At the end of the pumping period the complete system was degassed by heating (with a large flame) to about 300°C. After the system had cooled to room temperature, the furnace compartment was isolated by closing G and V_1, a krypton-xenon tracer was admitted and induction heating was started. The crucible

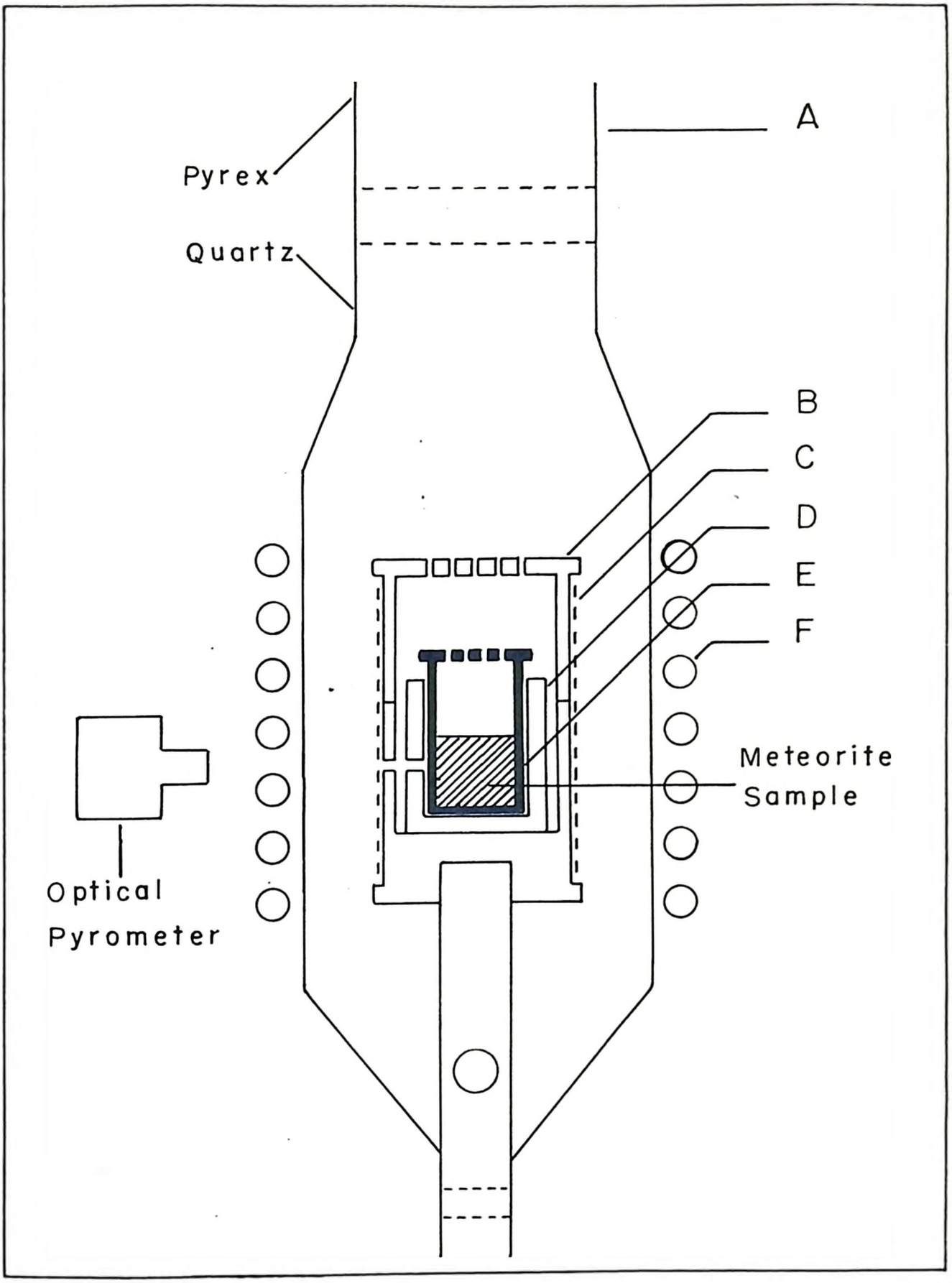

FIG. II-1 VACUUM INDUCTION FURNACE

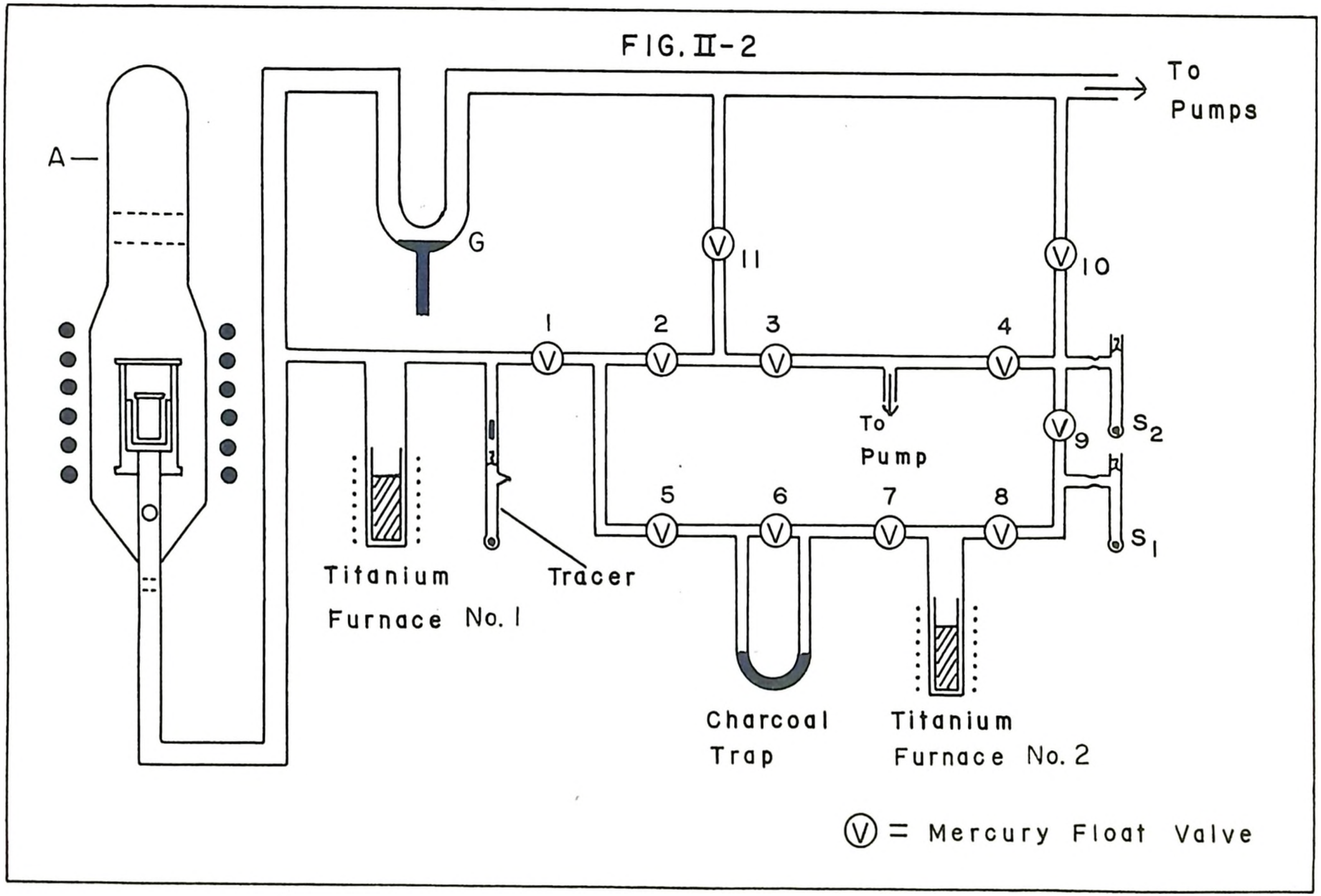

RARE GAS EXTRACTION & PURIFICATION SYSTEM

temperature, estimated by an optical pyrometer, was gradually raised to about 1600°C, and held there for 2 hours. During this time titanium furnace No. 1 was heated to 800°C. The hot titanium served to remove gases other than rare gases evolved from the meteorite. After extraction was complete, the gases were transferred to the charcoal trap, held at liquid nitrogen temperature, then with V_5 and V_8 closed, and V_6 and V_7 open, the temperature of the charcoal trap was raised to about 300°C, and the gas purified in titanium furnace No. 2. The residual gas, which consisted mainly of argon, krypton and xenon, was then transferred to the charcoal in S_1, held at liquid nitrogen temperature.

In order to test the completeness of extraction, fresh samples of meteorite were heated at temperatures in excess of 1600°C, for 4 - 6 hours. These tests indicated that, for each meteorite studied, a 1600°C heating for 2 hours resulted in at least 95% evolution of the rare gases.

3. Separation of Argon from Krypton and Xenon

During mass spectrometric analyses by the static method (see Part I, Section II, B 2b) it was found that if the argon was admitted to the sealed-off system with the krypton and xenon, systematic errors were introduced into isotope abundance measurements on krypton and xenon for the following reasons:

1. Argon was much more abundant than either krypton or xenon and caused ion beams of krypton and xenon to be scattered, thereby decreasing the resolution of the instrument.

2. Argon could cause an enhancement of the "memory effect" (see Part I, Section II, B 3b) for krypton and xenon.

3. The $(Kr^{80})^+$ peak was broadened by $(A^{40})^{++}$ ions which were reduced in charge to $(A^{40})^+$ ions by small-angle scattering between the ion source and the magnet pole.

The above effects can be reduced to negligible proportions by the separation of argon from krypton and xenon prior to analysis of krypton and xenon. The separation was accomplished by the following method:

After the argon-krypton-xenon mixture had been transferred to S_1 (Fig. II-2) at liquid nitrogen temperature, mercury float valves V_8, V_4 and V_{10} were closed and then with V_9 open, liquid nitrogen was placed on S_2, and the liquid nitrogen on S_1 replaced by freezing ethyl alcohol (-115°C). After 30 minutes, S_1 and S_2 were sealed off. It was found that after this procedure had been carried out, S_1 contained about 0.1% of the original argon, about 90% of the original krypton and about 99% of the original xenon. Tests carried out with mixtures of atmospheric argon, krypton and xenon, in approximately the same amounts as in the rare gas samples from meteorites, indicated that the isotopes of krypton and xenon were not fractionated to a measurable extent during the separation procedure.

4. Blank Determinations

During the extraction and purification procedures it is possible that serious contamination may arise from rare gases present in the air. In order to test this, blank determinations were carried out in which the procedures described in the previous sections were followed, except that there was no sample in the crucible. During blank determinations, about 10^{-10} cc STP of krypton and about 10^{-11} cc STP of xenon were collected. Since the stone meteorites studied in this work contained about 10^{-8} cc STP (for a 10-gm sample) of both krypton and xenon, the contamination error for krypton was about 1%, and about 0.1% for xenon.

It should be noted, however, that a blank determination only indicates the contamination arising from either the residual rare gases in the extraction and purification system, after degassing, or rare gases adsorbed on the walls of the system or on the crucible or crucible holder, to be released during the extraction and purification procedures. It is possible that part of the krypton and xenon collected during an extraction is adsorbed from the air during the terrestrial history of the meteorite prior to heating. This question will be discussed later in this thesis.

B. EXTRACTION OF RARE GASES FROM NATURAL GAS

The natural gases studied in this work contained about 0.1% of argon and only a few parts per billion of krypton and xenon. It was found that satisfactory removal of non-rare gases could be achieved by the use of three "getters", viz., titanium, calcium and uranium.

The apparatus used to obtain rare gas samples from natural gas is shown in Fig. II-3. Hydrogen and helium were removed by pumping the gas through the charcoal trap, held at liquid nitrogen temperature. The residue was then reacted with titanium heated to 800°C, calcium heated to 700°C and uranium filings heated to 700°C. Argon was separated from krypton and xenon by the procedure described previously.

C. MASS SPECTROMETRY AND ISOTOPE DILUTION

Samples of krypton and xenon obtained from stone meteorites were analysed by the static method (see Part I, Section II, B 2b). The isotope dilution method was used to determine the amounts of krypton and xenon evolved from the meteorite specimens (see Part I, Section II, A 1). Since the tracer isotopes Kr^{80}, Kr^{82} and Xe^{123} were present in meteoritic krypton

FIG. II-3

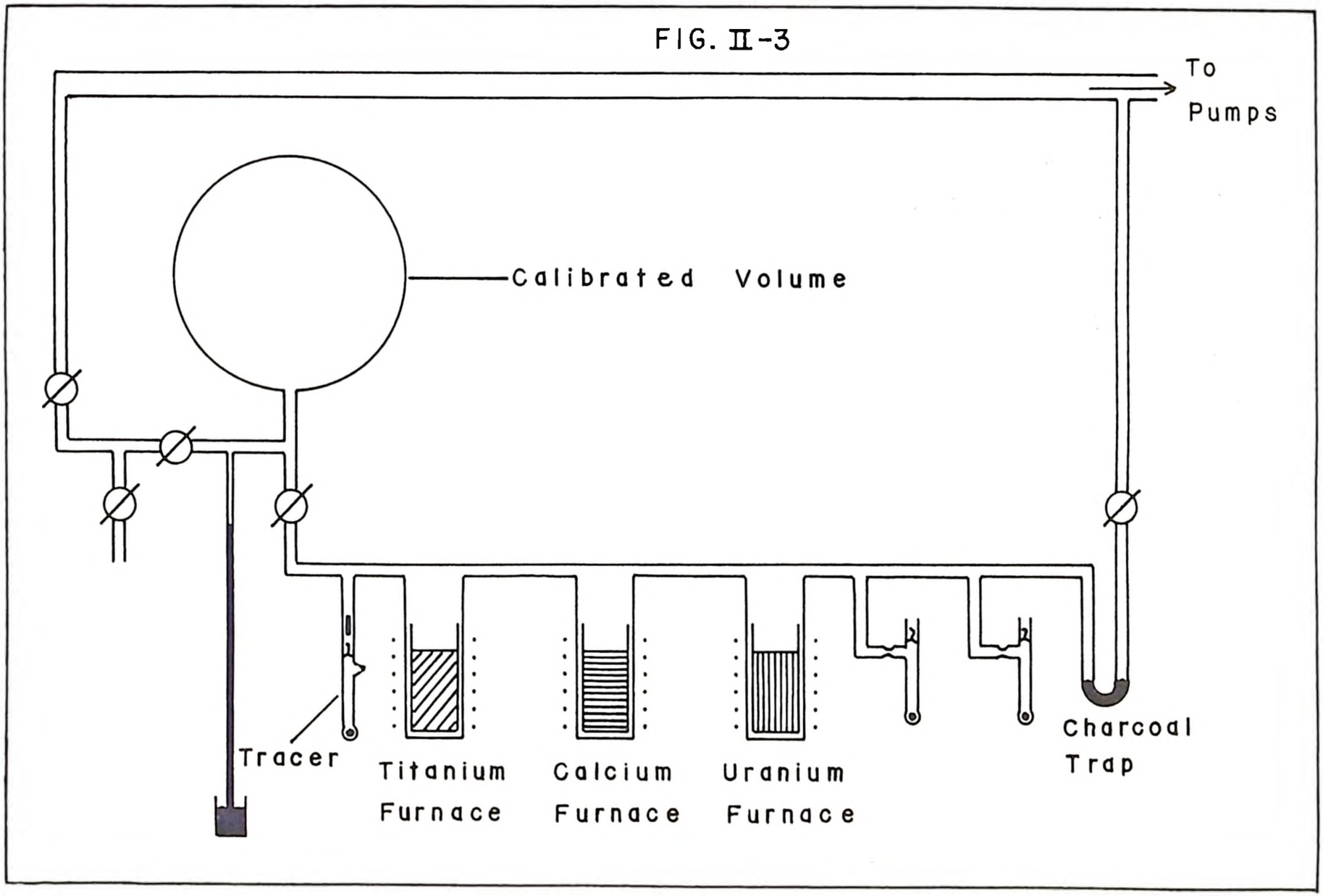

EXTRACTION SYSTEM FOR RARE GASES FROM NATURAL GAS

and xenon, two mass spectrometric analyses were necessary, one on meteoritic krypton and xenon mixed with a krypton-xenon tracer, and another analysis on krypton and xenon evolved from a fresh sample of meteorite with no tracer added during the extraction procedure.

Samples of krypton and xenon obtained from natural gas were analysed as described above. Argon samples obtained from natural gas were large compared to krypton and xenon samples and it was found that satisfactory isotopic abundance measurements could be obtained by means of the flow method (see Part I, Section II, B 2a). The tracer used for argon determinations was A^{36}, highly enriched by electromagnetic separation of atmospheric argon.

III. RESULTS

A. RARE GASES IN STONE METEORITES

1. Xenon

The results of mass spectrometric analyses of xenon evolved from four stone meteorites are presented in Tables II-I and II-II. Table II-I gives xenon isotope abundance data with the abundances normalised to $Xe^{130} = 1.000$. Table II-II gives the xenon contents of the meteorite specimens in cc STP/gm as determined by isotope dilution with Xe^{128} tracer.

Three separate samples of each meteorite were heated to obtain three samples of rare gas. Two of the rare gas samples were diluted with a krypton-xenon tracer and a third rare gas sample was undiluted. The first two rare gas samples were obtained using different heating conditions for the meteorite in order to test completeness of extraction (see Section II, A 2). Analyses of atmospheric xenon samples, of known Xe^{128} abundance carried out prior to the analyses of tracer undiluted samples, indicated that memory effects (see Part I, Section II, B 3b) for Xe^{128} were negligible. For each xenon sample analysed, 7 double mass spectrograms were taken. The xenon isotope abundances found for each sample from the same meteorite agreed to within the standard deviation of each set of 7 double mass spectrograms.

During the series of analyses of meteoritic xenon, seven standard samples of xenon were prepared from air by the same techniques used to purify gas evolved from the heated meteorites (see Sections II, A 2 and

TABLE II-I

Isotopic Composition of Xenon in the Stone Meteorites

Isotope	Bruderheim	Abee	Potter	La Lande
Xe^{124}	0.03107 ± 0.00020	0.02506 ± 0.00072	0.02470 ± 0.00031	0.02367 ± 0.00061
Xe^{126}	0.03214 ± 0.00021	0.02233 ± 0.00050	0.02350 ± 0.00030	0.02254 ± 0.00081
Xe^{128}	0.719 ± 0.015	0.548 ± 0.010	0.558 ± 0.004	0.668 ± 0.010
Xe^{129}	7.376 ± 0.028	39.5 ± 0.4	6.731 ± 0.039	6.806 ± 0.029
Xe^{130}	1.000	1.000	1.000	1.000
Xe^{131}	4.962 ± 0.019	5.032 ± 0.017	4.994 ± 0.039	5.070 ± 0.029
Xe^{132}	6.169 ± 0.020	6.210 ± 0.016	6.351 ± 0.048	6.377 ± 0.029
Xe^{134}	2.416 ± 0.009	2.366 ± 0.013	2.489 ± 0.012	2.507 ± 0.015
Xe^{136}	2.056 ± 0.011	1.987 ± 0.017	2.097 ± 0.010	2.120 ± 0.015

Note: Errors are standard deviations of 21 mass spectrograms for Xe^{124} .... etc., and of 7 mass spectrograms for Xe^{128}. The abundance data for Xe^{128} was obtained from measurements on tracer undiluted samples only.

TABLE II-II

Xenon Content of the Stone Meteorites

Meteorite	Xenon Content in cc STP/gm
Bruderheim	$1.00 \pm 0.03 \times 10^{-9}$
Abee	$7.5 \pm 0.2 \times 10^{-9}$
Potter	$1.08 \pm 0.03 \times 10^{-9}$
La Lande	$1.36 \pm 0.04 \times 10^{-9}$

II, A 3). The standard samples of xenon were approximately the same size as the meteoritic xenon samples and were analysed under the same operating conditions of the mass spectrometer. The results of mass spectrometric analyses of the atmospheric xenon samples are given in Table II-III. The average xenon isotope abundances of the seven atmospheric samples are used as comparison standards for the isotope abundances found for meteoritic xenon. Differences between the isotopic composition of atmospheric xenon and meteoritic xenon are expressed in the following way:

$$\delta_i = \left(\frac{Xe^i}{Xe^{130}}\right)_{\text{atmosphere}} - \left(\frac{Xe^i}{Xe^{130}}\right)_{\text{meteorite}}$$

Values of δ_i for xenon from the four stone meteorites studied in this work are given in Table II-IV. Fig. II-4 shows a tracing of the ion currents recorded during a single sweep of xenon from the Bruderheim meteorite, and illustrates the differences between the isotopic composition of atmospheric xenon and meteoritic xenon.

2. Krypton

The krypton evolved from the stone meteorites was also analysed and the results are given in Tables II-V and II-VI. Table II-V gives krypton isotope abundances normalised to $Kr^{86} = 1.000$. The atmospheric krypton isotope abundances given in the last column of Table II-V are average values of 5 analyses of atmospheric krypton prepared from aliquots of air in the same way the atmospheric xenon samples were prepared. The krypton isotope abundances were corrected for mass discrimination (see Part I, Section II, B 3a). Table II-VI gives the krypton contents of the meteorite specimens as determined by isotope dilution with Kr^{80} and Kr^{82} tracer. It is seen from Table II-V that there are significant differences

FIG.II-4 MASS SPECTROGRAM OF XENON FROM THE BRUDERHEIM METEORITE

------- ATMOSPHERIC XENON ISOTOPE PATTERN

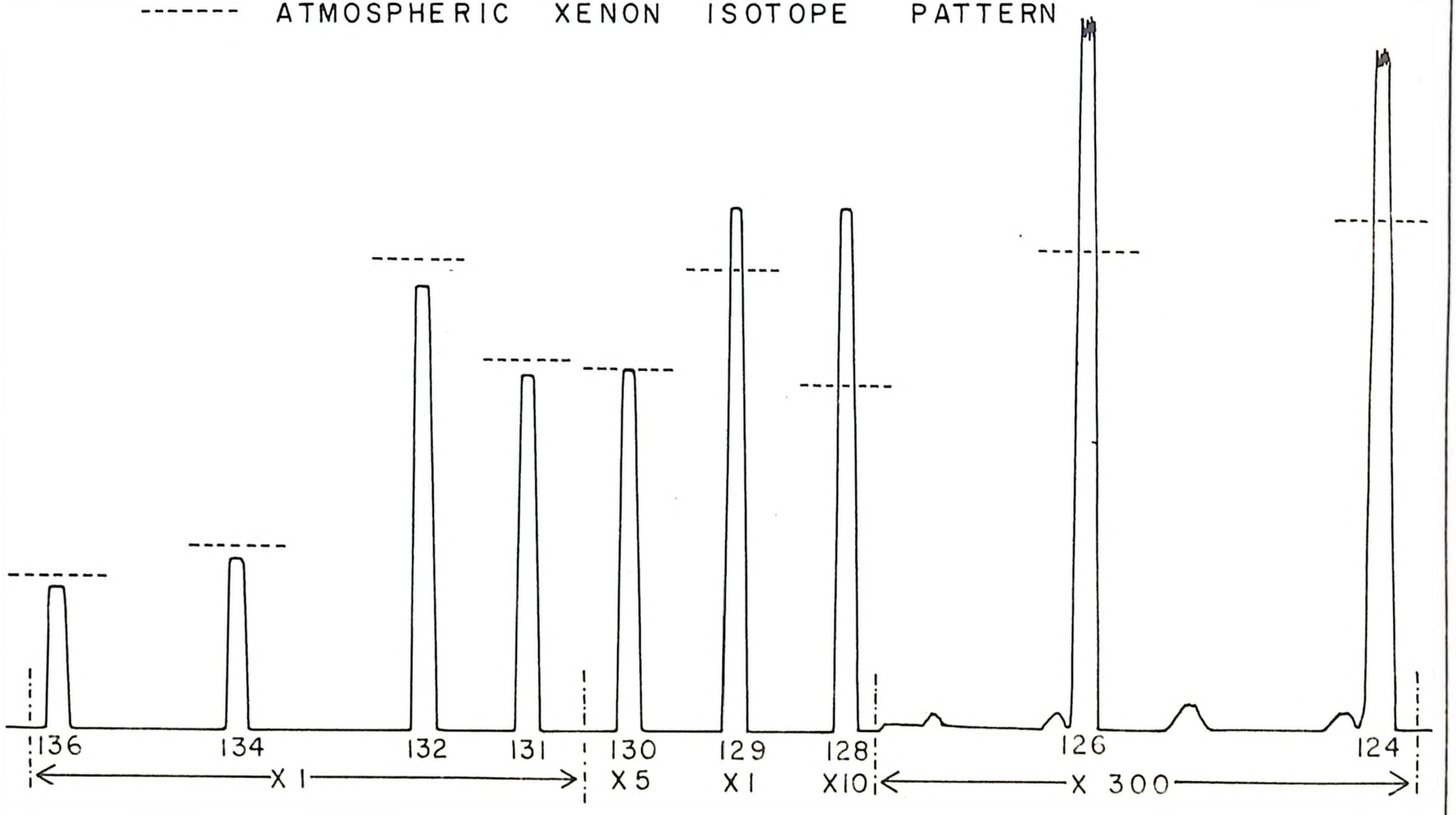

TABLE II-III

Isotopic Analyses of Atmospheric Xenon Samples

Sample No.	Atom Percent								
	Xe^{124}	Xe^{126}	Xe^{128}	Xe^{129}	Xe^{130}	Xe^{131}	Xe^{132}	Xe^{134}	Xe^{136}
1	0.0959	0.0899	1.883	26.60	4.098	21.08	26.92	10.37	8.865
2	0.0966	0.0900	1.928	26.39	4.093	21.16	26.86	10.48	8.905
3	0.0970	0.0900	1.936	26.57	4.109	21.09	26.81	10.41	8.870
4	0.0975	0.0910	1.940	26.54	4.120	21.18	26.83	10.38	8.829
5	0.0973	0.0898	1.941	26.60	4.121	21.12	26.78	10.41	8.840
6	0.0968	0.0897	1.932	26.52	4.103	21.20	26.82	10.36	8.873
7	0.0971	0.0901	1.938	26.61	4.115	21.11	26.77	10.39	8.868
Average	0.0968 ± 0.0005	0.0901 ± 0.0004	1.928 ± 0.019	26.55 ± 0.09	4.108 ± 0.009	21.13 ± 0.05	26.83 ± 0.05	10.40 ± 0.04	8.864 ± 0.023
Average Abundances Normalised to Xe^{130} = 1.000	0.02356 ± 0.00017	0.02193 ± 0.00014	0.469 ± 0.006	6.463 ± 0.036	1.000	5.144 ± 0.024	6.531 ± 0.027	2.532 ± 0.016	2.158 ± 0.010

TABLE II-IV

Comparison of the Isotopic Composition of Atmospheric Xenon and Xenon from the Meteorites

$$\delta_i = \left(\frac{Xe^i}{Xe^{130}}\right)_{\text{atmosphere}} - \left(\frac{Xe^i}{Xe^{130}}\right)_{\text{meteorite}}$$

δ_i	Bruderheim	Abee	Potter	La Lande
δ_{124}	- 0.0075 ± 0.004	- 0.0015 ± 0.0009	- 0.0011 ± 0.0005	- 0.0001 ± 0.0008
δ_{126}	- 0.0102 ± 0.0003	- 0.0004 ± 0.0005	- 0.0016 ± 0.0004	- 0.0006 ± 0.0009
δ_{128}	- 0.250 ± 0.008	- 0.079 ± 0.007	- 0.089 ± 0.010	- 0.199 ± 0.07
δ_{129}	- 0.91 ± 0.06	- 33.0 ± 0.5	- 0.27 ± 0.07	- 0.34 ± 0.07
δ_{130}	≡ 0	≡ 0	≡ 0	≡ 0
δ_{131}	+ 0.18 ± 0.04	+ 0.11 ± 0.04	+ 0.15 ± 0.06	+ 0.07 ± 0.05
δ_{132}	+ 0.36 ± 0.05	+ 0.32 ± 0.04	+ 0.18 ± 0.07	+ 0.15 ± 0.06
δ_{134}	+ 0.12 ± 0.03	+ 0.17 ± 0.03	+ 0.04 ± 0.03	+ 0.03 ± 0.03
δ_{136}	+ 0.10 ± 0.02	+ 0.17 ± 0.03	+ 0.06 ± 0.02	+ 0.04 ± 0.02

TABLE II-V

Isotopic Composition of Krypton in the Stone Meteorites and in the Atmosphere

Isotope	Bruderheim	Abee	Potter	La Lande	Atmosphere
Kr^{78}	0.0272 ± 0.0005	0.0201 ± 0.0002	0.0219 ± 0.0003	0.0192 ± 0.0006	0.0204 ± 0.0002
Kr^{80}	0.157 ± 0.004	0.187 ± 0.003	0.133 ± 0.002	0.129 ± 0.003	0.131 ± 0.001
Kr^{82}	0.716 ± 0.004	0.681 ± 0.003	0.672 ± 0.004	0.672 ± 0.004	0.669 ± 0.003
Kr^{83}	0.725 ± 0.003	0.661 ± 0.003	0.670 ± 0.005	0.665 ± 0.003	0.666 ± 0.002
Kr^{84}	3.324 ± 0.022	3.259 ± 0.028	3.258 ± 0.012	3.271 ± 0.018	3.286 ± 0.015
Kr^{86}	1.000	1.000	1.000	1.000	1.000

TABLE II-VI

Krypton Content of the Stone Meteorites

Meteorite	Krypton Content in cc STP/gm
Bruderheim	$0.23 \pm 0.3 \times 10^{-9}$
Abee	$1.2 \pm 0.2 \times 10^{-9}$
Potter	$0.76 \pm 0.20 \times 10^{-9}$
La Lande	$0.68 \pm 0.15 \times 10^{-9}$

between the isotope abundances of meteoritic krypton and atmospheric krypton only for the Bruderheim and Abee meteorites, with a possible excess of Kr^{78} for krypton from the Potter meteorite.

B. RARE GASES IN NATURAL GAS

1. Description of the Samples

The natural gas samples studied in this work were obtained from the U. S. Bureau of Mines. They were collected in ordinary stainless steel gas cylinders, which were well purged of air before filling. The source of each sample, as well as pertinent sampling data, is given in Table II-VII.

2. Xenon

Fig. II-5 shows a tracing of ion currents recorded during a single sweep of the spectrum of xenon from Navajo natural gas, and shows the existence of definite differences between the isotopic composition of xenon from natural gas, and xenon from the atmosphere. Differences between the two types of xenon are written in terms of δ_i values where δ_i is defined as follows:

$$\delta_i = \left(\frac{Xe^i}{Xe^{130}}\right)_{\text{natural gas}} - \left(\frac{Xe^i}{Xe^{130}}\right)_{\text{atmosphere}}$$

Values of δ_i for xenon from the natural gas sources, arranged in order of increasing helium content, are given in Table II-VIII.

3. Krypton

The abundance of the krypton isotopes was measured for all four natural gas sources. It was found that the isotopic composition of krypton from natural gas was identical, within the errors of the measurements, to the isotopic composition of atmospheric krypton. It will be shown later that the differences between the xenon isotope patterns in

FIG.II-5 MASS SPECTROGRAM OF XENON FROM NAVAJO NATURAL GAS

------- ATMOSPHERIC XENON ISOTOPE PATTERN

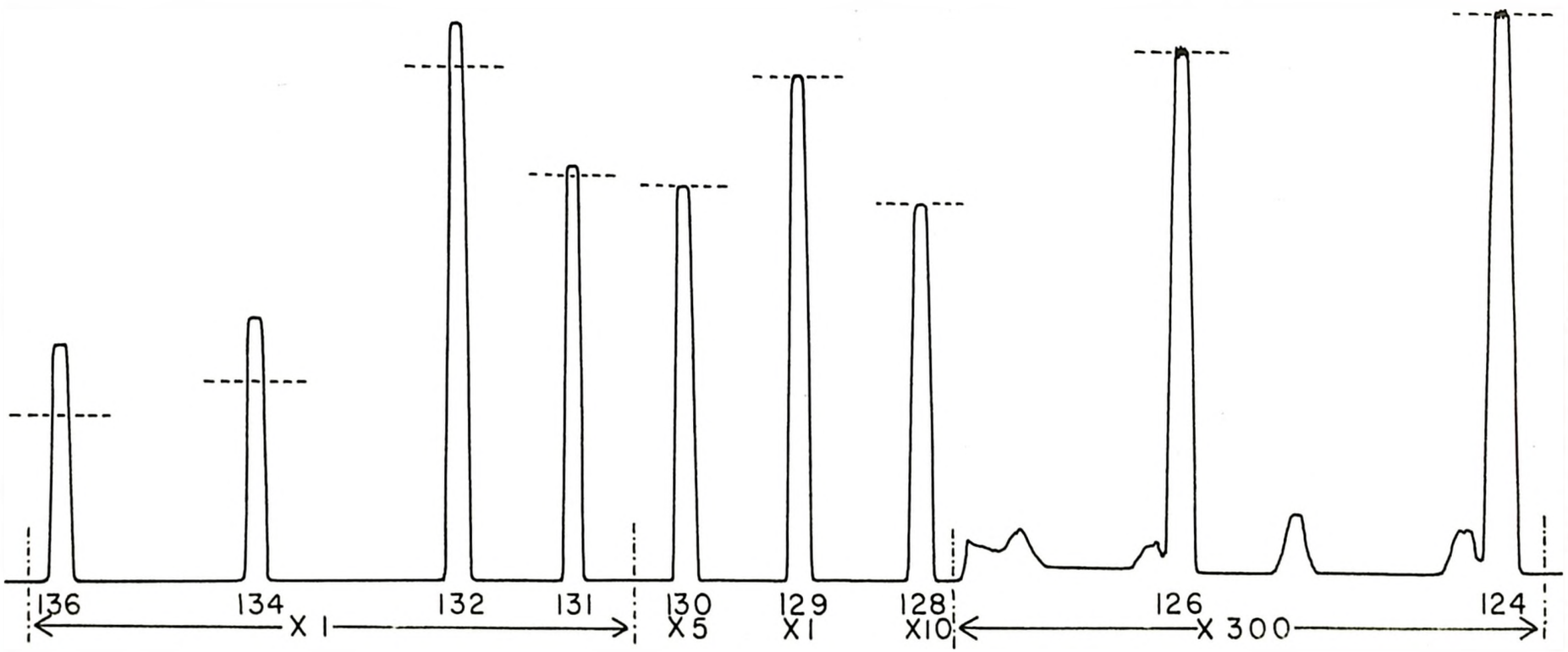

TABLE II-VII

Location and Description of Natural Gas Samples

Location	Date Sampled	Sampling Pressure - psig	He%
Panoma Plant, East Panhandle Field, Texas	December 28, 1961	610	0.27
Channing Well, West Panhandle Field, Texas	June 11, 1954	500	1.0
Cliffside Well, West Panhandle Field, Texas	June 10, 1954	500	1.8
Navajo C-1 Well, Wildcat Field, New Mexico	January 5, 1962	410	5.7

TABLE II-VIII

Comparison of the Isotopic Composition of Xenon
in Natural Gas with Xenon in the Atmosphere

$$\delta_i = \left(\frac{Xe^i}{Xe^{130}}\right)_{\text{natural gas}} - \left(\frac{Xe^i}{Xe^{130}}\right)_{\text{atmosphere}}$$

δ_i	Panoma	Channing	Cliffside	Navajo
δ_{124}	+ 0.0003 ± 0.0003	+ 0.0002 ± 0.0003	+ 0.0001 ± 0.0002	- 0.0002 ± 0.0004
δ_{126}	+ 0.0002 ± 0.0003	- 0.0002 ± 0.0003	- 0.0001 ± 0.0003	- 0.0001 ± 0.0004
δ_{128}	+ 0.002 ± 0.003	+ 0.001 ± 0.005	+ 0.0002 ± 0.0003	- 0.004 ± 0.004
δ_{129}	+ 0.01 ± 0.04	- 0.02 ± 0.02	+ 0.01 ± 0.02	+ 0.03 ± 0.02
δ_{130}	≡ 0	≡ 0	≡ 0	≡ 0
δ_{131}	+ 0.03 ± 0.03	+ 0.03 ± 0.02	+ 0.03 ± 0.03	+ 0.12 ± 0.03
δ_{132}	+ 0.02 ± 0.03	+ 0.07 ± 0.02	+ 0.07 ± 0.02	+ 0.46 ± 0.03
δ_{134}	+ 0.01 ± 0.02	+ 0.06 ± 0.01	+ 0.07 ± 0.02	+ 0.47 ± 0.01
δ_{136}	- 0.01 ± 0.02	+ 0.08 ± 0.02	+ 0.07 ± 0.02	+ 0.57 ± 0.01

natural gas and the atmosphere are caused by spontaneous fission of U^{238}. The failure to find similar differences for the krypton isotope patterns is not surprising, for the following reasons:

1. Krypton is about ten times more abundant than xenon in natural gas.

2. The yield of krypton in spontaneous fission of U^{238} is only about one-tenth the yield of xenon.

4. Argon

The argon isotopes in the natural gas sources were examined, and the abundances are given in Table II-IX. The abundance pattern of the argon isotopes in the atmosphere is given for comparison. It is seen that while A^{36} and A^{38} are nearly the same in all cases, A^{40} is greatly enriched in natural gas, due to radioactive decay of K^{40}.

5. Rare Gas Contents

The rare gas contents of the four natural gas sources, as determined by isotope dilution with A^{36}, Kr^{80}, Kr^{82} and Xe^{128} are given in Table II-X.

TABLE II-IX

The Isotopic Composition of Argon in Natural Gas and in the Atmosphere

Source	A^{40}/A^{36}	A^{38}/A^{36}
Panoma	930 ± 20	0.194 ± 0.003
Channing	1810 ± 20	0.194 ± 0.007
Cliffside	1780 ± 30	0.186 ± 0.006
Navajo	30000 ± 5000	0.177 ± 0.021
Atmosphere	293	0.185

TABLE II-X

The Rare Gas Contents of Natural Gas and the Atmosphere

Source	He %	A of Air Composition %	A of Radiogenic Composition %	Kr %	Xe %
Panoma	0.27	0.0063	0.0135	1.48×10^{-6}	3.34×10^{-7}
Channing	1.0	0.020	0.106	4.18×10^{-6}	3.36×10^{-7}
Cliffside	1.8	0.026	0.137	4.10×10^{-6}	3.27×10^{-7}
Navajo	5.7	0.0060	0.58	1.06×10^{-6}	2.04×10^{-7}
Atmosphere	4×10^{-3}	0.94	.....	3.2×10^{-4}	2.5×10^{-5}

Note: The error for all rare gas contents is less than 10%.

IV. DISCUSSION

A. XENON AND KRYPTON IN STONE METEORITES

It is seen from the data given in Table II-IV that there is a definite pattern in the differences in isotopic composition of xenon from stone meteorites and xenon from the atmosphere. Firstly, there is a large excess of Xe^{129} in meteoritic xenon; secondly, meteoritic xenon contains an excess of the isotopes of xenon "shielded" in fission, viz., Xe^{124}, Xe^{126} and Xe^{128}, and thirdly, atmospheric xenon contains an excess of the isotopes of xenon chiefly produced in fission, viz., Xe^{131}, Xe^{132}, Xe^{134} and Xe^{136}. These three features will be discussed in turn.

1. The Xe^{129} Anomaly

Assuming that the Xe^{129} anomaly is a result of the *in situ* decay of extinct I^{129} (Jeffery and Reynolds 1961), the I^{129}-Xe^{129} decay interval, or the time interval between the end of element synthesis and the beginning of retention of xenon for a particular meteorite, can be calculated provided the iodine content of the meteorite specimen is known. Wasserburg et al (1960) have given the following relation:

$$\ln\left(\frac{I^{127}}{Xe_r^{129}}\right) = \frac{\Delta t}{\tau} + \ln\left(\frac{T}{\tau}\right) + \ln\left(\frac{K_{127}}{K_{129}}\right)$$

where Δt is the I^{129}-Xe^{129} decay interval

I^{127} is the iodine content of the meteorite

Xe_r^{129} is the content of "excess" Xe^{129} in the meteorite

τ is the mean life of I^{129}

T is the duration of nucleosynthesis

and K_{127} and K_{129} are production rates of I^{127} and I^{129} during nucleosynthesis

A derivation of the above expression is given in Appendix B.

Anders (1962) has made the following assumptions:

1. The "excess" Xe^{129} content may be calculated from the Xe^{129}/Xe^{130} ratio in the meteorite, the Xe^{129}/Xe^{130} ratio in the atmosphere, and the xenon content of the meteorite.

2. $T = 10^{10}$ years.

3. $K_{127} = K_{129}$.

The iodine contents of the Bruderheim and Abee meteorites have been measured by Goles and Anders (1962). Hence the I^{129}-Xe^{129} decay intervals (Δt) for the Bruderheim and Abee meteorites may be calculated. Table II-XI gives a compilation of data on meteorites for which the iodine and xenon contents are known. It is interesting to note that the I^{129}-Xe^{129} decay intervals for meteorites with very different textures and iodine contents appear to be the same within experimental error.

2. The Shielded Anomalies

It is apparent from the data given in Table II-IV that some process has added the light shielded isotopes to meteoritic xenon to a greater extent than to atmospheric xenon. Goles and Anders (1961) have suggested that since the abundances of Xe^{124} and Xe^{126} are so low as compared to the other isotopes of xenon, they will be most strongly affected by spallation reactions on nuclides of $A \geqslant 127$. The anomaly in Xe^{128} could in part be caused by spallation reactions on nuclides of $A \geqslant 129$, and in

TABLE II-XI

Xenon and Iodine Contents of Stone Meteorites
and I^{129}-Xe^{129} Decay Intervals

Meteorite	I ppb	Xe^{129}/Xe^{130}	Xenon Content cc STP/gm x 10^{-9}	Δt (Million Years)
Bruderheim	16 ± 6*	7.38 ± 0.03	1.00 ± 0.03	122 ± 12
Abee	145 ± 24*	39.5 ± 0.4	7.5 ± 0.02	116 ± 4
Indarch	270 ± 45*	19.1 ± 1.1**	6.5**	91 ± 12**
Murray	230 ± 50*	6.48 ± 0.03Δ	43Δ	..... †
Richardton	28 ± 4*	8.99 ± 0.05 †	1.04 †	113 ± 4**

*Goles and Anders (1962)

**Anders (1962)

ΔReynolds (1960b)

† Reynolds (1960a)

‡ Since the Xe^{129} anomaly is zero, a calculation of Δt is impossible

part by neutron capture in I^{127}. Krummenacher et al (1962) have proposed that the shielded anomalies are caused by strong mass fractionation of terrestrial xenon, leading to a depletion of the light isotopes. This mechanism requires that the heavy isotopes $Xe^{131-136}$ are correspondingly enriched in atmospheric xenon. However, mass fractionation alone cannot explain the anomalies in $Xe^{131-136}$ since this hypothesis leads to larger δ_i values for $Xe^{131-136}$ than are actually observed. Krummenacher et al proposed that fission-product xenon was added to meteoritic xenon (in an unspecified way) in order to remove this difficulty.

The mechanism proposed by Goles and Anders seems more plausible than the mechanism proposed by Krummenacher et al for the following reasons:

1. Bruderheim and Abee have similar values for the anomalies in $Xe^{131-136}$, but markedly different anomalies in $Xe^{124-128}$ (Table II-IV). It is possible that anomalies in $Xe^{124-128}$ and $Xe^{131-136}$ for Potter and La Lande are decreased because of atmospheric contamination.

2. Atmospheric krypton apparently shows little effect of strong mass fractionation (this is discussed in Section 4).

For the purpose of the discussion in the following section, it will be assumed that the shielded anomalies are caused by some type of nuclear process which affected meteoritic matter to a greater extent than terrestrial matter, and that the anomalies in $Xe^{131-136}$ are caused by some type of nuclear process which affected terrestrial xenon to a greater extent than meteoritic xenon.

3. The Fission Anomalies

Kuroda (1960) has shown that spontaneous fission of U^{238} during the entire history of the earth (4.5×10^9 years), even assuming complete degassing of the earth, can account for no more than 1% of the observed anomalies in the fission-produced isotopes of xenon. Kuroda proposed that the spontaneous fission of an extinct transuranium element such as Pu^{244} ($T_{1/2} = 7.6 \times 10^7$ y) in the early history of the earth could well account for the fission anomalies. It has been pointed out by Goles and Anders (1961) that the effect is more prominent for the earth's atmosphere than for the meteorites because the xenon content per gram of the earth (assuming that atmospheric xenon represents the total xenon in the earth system) is quite low compared to the xenon content in stone meteorites. For example, the xenon content of the earth, making the above assumption, is about 7×10^{-11} cc STP/gm as compared to 1×10^{-9} - 4×10^{-8} cc STP/gm for the meteorites.

Although it will be shown later in this thesis that the assumption that atmospheric xenon represents the total xenon in the earth system may not be valid, it is of interest to test Kuroda's hypothesis by comparing δ_i values for $Xe^{131-136}$ with the spontaneous fission mass-yield curve for Pu^{244}. However, the mass-yield curve for Pu^{244} is not available in the literature and the best that can be done is to use the three available mass-yield curves for the spontaneous fission of U^{238} (Ashizawa and Kuroda 1957; Young and Thode 1960), Cm^{242} (Steinberg and Glendenin 1954) and Cf^{252} (Steinberg and Glendenin 1955). Table II-XII gives δ_i values for $Xe^{131-136}$ for the four meteorites studied in this work as well as δ_i values for four meteorites studied by Krummenacher et al (1962).

TABLE II-XII

The Fission Anomalies
Values of δ_i/δ_{136} for Xenon from the Meteorites

$$\frac{\delta_i}{\delta_{136}} = \frac{\left(\frac{Xe^i}{Xe^{130}}\right)_{atmosphere} - \left(\frac{Xe^i}{Xe^{130}}\right)_{meteorite}}{\left(\frac{Xe^{136}}{Xe^{130}}\right)_{atmosphere} - \left(\frac{Xe^{136}}{Xe^{130}}\right)_{meteorite}}$$

Meteorite	Mass Number			
	131	132	134	136
Bruderheim	1.8 ± 0.4	3.6 ± 0.5	1.2 ± 0.3	1.0 ± 0.2
Abee	0.6 ± 0.2	1.0 ± 0.2	1.0 ± 0.2	1.0 ± 0.2
Potter	2.5 ± 1.0	3.0 ± 1.2	0.7 ± 0.5	1.0 ± 0.3
La Lande	1.7 ± 1.2	3.7 ± 1.5	0.7 ± 0.7	1.0 ± 0.5
*Murray	0.8 ± 0.2	2.3 ± 0.3	1.1 ± 0.1	1.0 ± 0.1
*Mighei	0.7 ± 0.4	2.3 ± 0.6	1.3 ± 0.2	1.0 ± 0.1
*Orgueil	0.6 ± 0.2	2.2 ± 0.3	1.1 ± 0.1	1.0 ± 0.1
*Richardton	0.8 ± 0.5	2.3 ± 0.7	0.9 ± 0.3	1.0 ± 0.3
Average	0.9 ± 0.3	2.4 ± 0.4	1.1 ± 0.1	1.0 ± 0.2

*Krummenacher et al (1962)

Although the above authors have examined the isotopic composition of xenon from several other meteorites, they consider that the analyses of xenon from the four meteorites given in Table II-XII are the most reliable, because of the small possibility of atmospheric contamination. It has been stated previously that the possibility of atmospheric contamination of the xenon samples during extraction is negligible (see Section II, A 4). However, there is a possibility of atmospheric contamination during the terrestrial history of the meteorite. In this connection it is noted that Bruderheim (fell 1960) and Abee (fell 1951) have larger δ_1 values (Table II-IV) than Potter (found 1941) or La Lande (found 1933).

Hence, in calculating the average values given in Table II-XII, only data for the Bruderheim and Abee meteorites, and data from the four meteorites studied by Krummenacher et al (1962) was used. Fig. II-6 shows a comparison of the average relative fission yields given in Table II-XII and the mass-yield curves for spontaneous fission of U^{238}, Cm^{242} and Cf^{252}. It appears that there are discrepancies at masses 131 and 132, with a more marked discrepancy at mass 132. In a similar comparison, Kuroda (1960) noted the marked discrepancy at mass 132 and attributed this tentatively to fine structure in the mass-yield curve of Pu^{244} spontaneous fission. However, fine structure of this magnitude has never been observed in mass-yield curves either of spontaneous fission, or particle induced fission of heavy elements. Moreover, mass-yield curves for spontaneous fission appear to have the following characteristics:

1. They are of the asymmetric type.

2. The position of the high mass peak appears to be relatively unchanged with the mass of the fissioning nuclide.

FIG. II-6

COMPARISON OF FISSION YIELDS OF THE FISSION-PRODUCT COMPONENT OF XENON IN THE ATMOSPHERE WITH THE YIELDS IN SPONTANEOUS FISSION OF U^{238}, Cf^{252}, AND Cm^{242}.

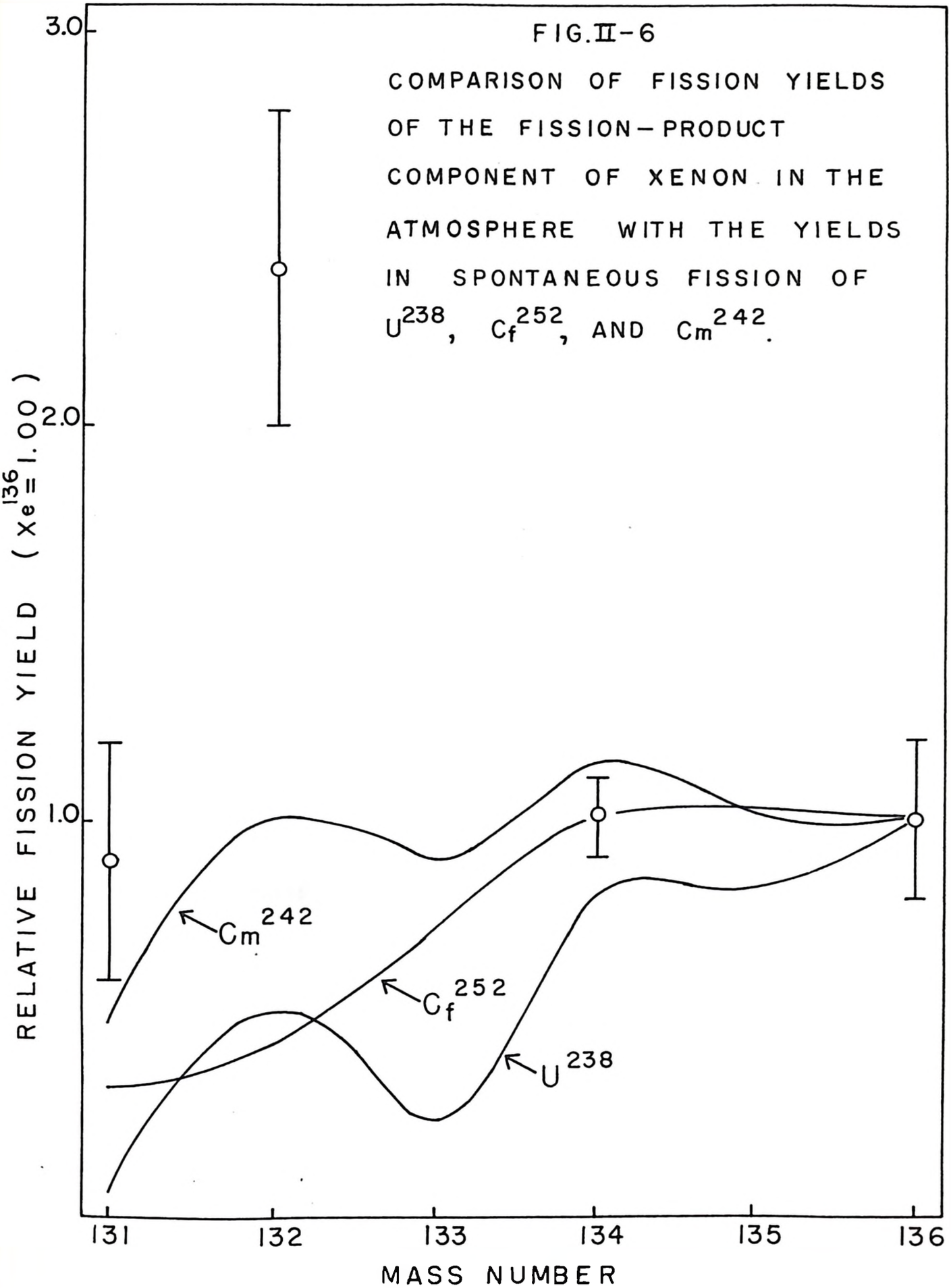

3. The yields decline rather sharply from the maximum yield (at about mass 140) to mass 131.

An alternative explanation of the discrepancies at masses 131 and 132 might be the fractionation phenomenon that occurs when fission-product xenon diffuses from fissile material. For example, large isotope enrichments are observed for Xe^{131} and Xe^{132} in low temperature fractions of xenon evolved from uranium oxide powders (Kennett and Thode 1960; Part I of this thesis). The isotope enrichments were observed in xenon released below 500°C, and this xenon was only a small fraction ($<$ 1%) of the total available xenon in the system. Hence the explanation of the discrepancies at masses 131 and 132 requires that only a small fraction of the available xenon from spontaneous fission of Pu^{244} be present in the atmosphere. It is possible to arrive at a limiting value by the following argument:

It is seen from Fig. II-6 that the fission yield of Xe^{132} is at least a factor of 2 higher than the fission yields of Xe^{131}, Xe^{134} or Xe^{136}. If it is assumed that <u>all</u> the available fission-product Xe^{132} is presently in the atmosphere, then it must be concluded that only about 50% of the available Xe^{131}, Xe^{134} and Xe^{136} are presently in the atmosphere. Thus, the atmosphere contains about 60% of the total available fission-product xenon. However, complete separation of Xe^{132} from the other isotopes of xenon produced in fission by the mechanism of diffusion and decay of xenon precursors is extremely unlikely. The actual percentage of available fission-product xenon in the atmosphere would more likely be much lower than 60%. In this connection it is noted that there are two conflicting views regarding the degassing of the earth:

1. Damon and Kulp (1958) have shown that the present rate of entry of A^{40} into the atmosphere from the crust is far too small to account for the A^{40} content in the atmosphere at the present time. They concluded that there was a major degassing of the interior of the earth approximately 3.5×10^9 years ago. The way in which Damon and Kulp calculated a value for the rate of entry of A^{40} from the crust into the atmosphere was as follows:

The estimated cosmic ray production rate of He^3, and its abundance in the atmosphere, was used to calculate the rate of loss of He^4 from the atmosphere and, hence, the rate of entry of He^4 into the atmosphere from the earth's crust, assuming that steady state conditions have been established. The rate of entry of He^4 is then used to calculate the rate of entry of A^{40}.

2. Turekian (1959) has challenged the view of Damon and Kulp because of the uncertainties in the estimates of He^3 cosmic ray production rate. Turekian considered the total earth to be of chondritic composition (i.e., has the same content of potassium as the average value for stone meteorites) and used the known abundance of A^{40} in the atmosphere, and a model of continuous degassing of the earth. He concluded that only about 10% of the A^{40} formed in the solid earth over the last 5.0×10^9 years is present in the atmosphere now, and that in the first 500 million years of the earth's history only about 6% of the A^{40} formed entered the atmosphere.

The fact that the mechanism of diffusion and decay of fission-product xenon precursors can explain the observed discrepancies at Xe^{131} and Xe^{132} only if a small fraction of the available fission-product xenon

has diffused into the atmosphere supports the view of Turekian. According to his view, there was no major degassing of the earth either in its early history, or since. This is a conclusion which supports the arguments of Urey (1952) who considers that the accumulation of the planets was a low temperature process.

4. The Krypton Anomalies

One might expect to find anomalies in krypton similar to those found for xenon, i.e. evidence of a meteoritic excess of the shielded isotopes of krypton (Kr^{78}, Kr^{80} and Kr^{82}) and evidence of an atmospheric excess of the krypton isotopes chiefly produced in fission (Kr^{83}, Kr^{84} and Kr^{86}). It can be predicted that the effects for Kr^{83-86} would be much smaller than the effects for $Xe^{131-136}$. For example, if the fission yields of Xe^{136} and Kr^{86} are assumed to be 6% and 1% respectively, then since the krypton-xenon ratio in the atmosphere is about 15, a 10% fission component in Xe^{136} corresponds to only a 0.1% fission component in Kr^{86}.

From the krypton data given in Table II-V, with the krypton isotope abundances normalised to $Kr^{86} = 1.000$, the following facts are apparent:

1. Bruderheim krypton contains excess Kr^{78}, Kr^{80}, Kr^{82} and Kr^{83}.
2. Abee krypton contains excess Kr^{80}.
3. Potter krypton contains excess Kr^{78}.

The above discrepancies are quite definite and exceed the experimental error by a factor of 3 to 10. Krummenacher et al (1962) have examined the isotopic composition of krypton from several meteorites and found no certain differences between the isotopic composition of meteoritic krypton and atmospheric krypton, except for a possible excess of Kr^{86} in

the Richardton meteorite and a possible deficiency in Kr^{82} for the Orgueil and Murray meteorites.

Even though the expected amount of fission-product krypton in the atmosphere would be negligible, a superficial examination of the Bruderheim krypton data appears to indicate fission-product krypton in the atmosphere. If the Bruderheim and atmosphere krypton isotope patterns are normalised to the shielded isotope Kr^{82}, then a subtraction of the meteoritic krypton isotope pattern from the atmospheric krypton isotope pattern gives the following "fission yields" (normalised to yield of $Kr^{86} = 1.0$):

Atmosphere - Bruderheim - $Kr^{83} = -0.17 \pm 0.07$, $Kr^{84} = 2.7 \pm 0.5$

These are, of course, extraordinary fission yields. The fission yields of Kr^{86-83} in spontaneous fission decrease sharply from Kr^{86} to Kr^{83}. From the above comparison it would appear that the yield of Kr^{84} is at least twice the yield of Kr^{86}. In this case the yield discrepancy cannot be explained by the mechanism used to account for the Xe^{131} and Xe^{132} yield discrepancies in the fission-product xenon in the atmosphere, since no abnormal isotope effects are found for the diffusion of fission-product krypton from fissile material (Part I).

The possibility of fission-product krypton in the atmosphere would therefore appear to be small for the following reasons:

1. The expected amount of fission-product krypton is only about 1% of the expected amount of fission-product xenon.

2. Although Bruderheim krypton appears to have excess Kr^{84} and Kr^{86} (based on a Kr^{82} normalisation of the meteoritic and atmospheric krypton isotope patterns), the yield ratio of Kr^{84}/Kr^{86} is abnormally large.

3. There is no supporting evidence of an atmospheric fission-product component from the krypton data for the other meteorites.

The question arises as to whether the krypton anomalies (for Bruderheim) could have been caused by mass fractionation of terrestrial krypton, leading to a depletion of the light isotopes. Fig. II-7 shows a plot of $\log_{10}\left[(Kr^{i}/Kr^{86})_{meteoritic}/(Kr^{i}/Kr^{86})_{atmospheric}\right]$ versus $\sqrt{M}$. It is seen that a straight line will not fit all the points in the plot. Moreover, there is no supporting evidence for mass fractionation from the krypton data for the other meteorites. For example, the Kr^{80} anomaly is larger for Abee krypton than for Bruderheim krypton and yet there are insignificant anomalies in the other isotopes of Abee krypton.

The krypton anomalies are more likely explained by nuclear processes which affected meteoritic matter to a greater extent than terrestrial matter. For example, the anomaly in Kr^{78} might be explained by spallation reactions, a mechanism used by Goles and Anders (1961) to explain the anomalies in the shielded isotopes Xe^{124} and Xe^{126}. In this connection it may be noted that Bruderheim contains the largest excess of Kr^{78}, and also the largest excess of Xe^{124} and Xe^{126} for the meteorites studied in this work. Anomalies in Kr^{80} and Kr^{82} may possibly be explained by n-γ reactions on Br^{79} and Br^{81}.

B. RARE GASES IN NATURAL GAS

1. <u>The Normal Rock Hypothesis</u>

It is seen from Table II-VIII that xenon from natural gas of high helium content contains an excess of the isotopes produced chiefly in fission, viz., $Xe^{131-136}$, as compared to xenon from the atmosphere. The

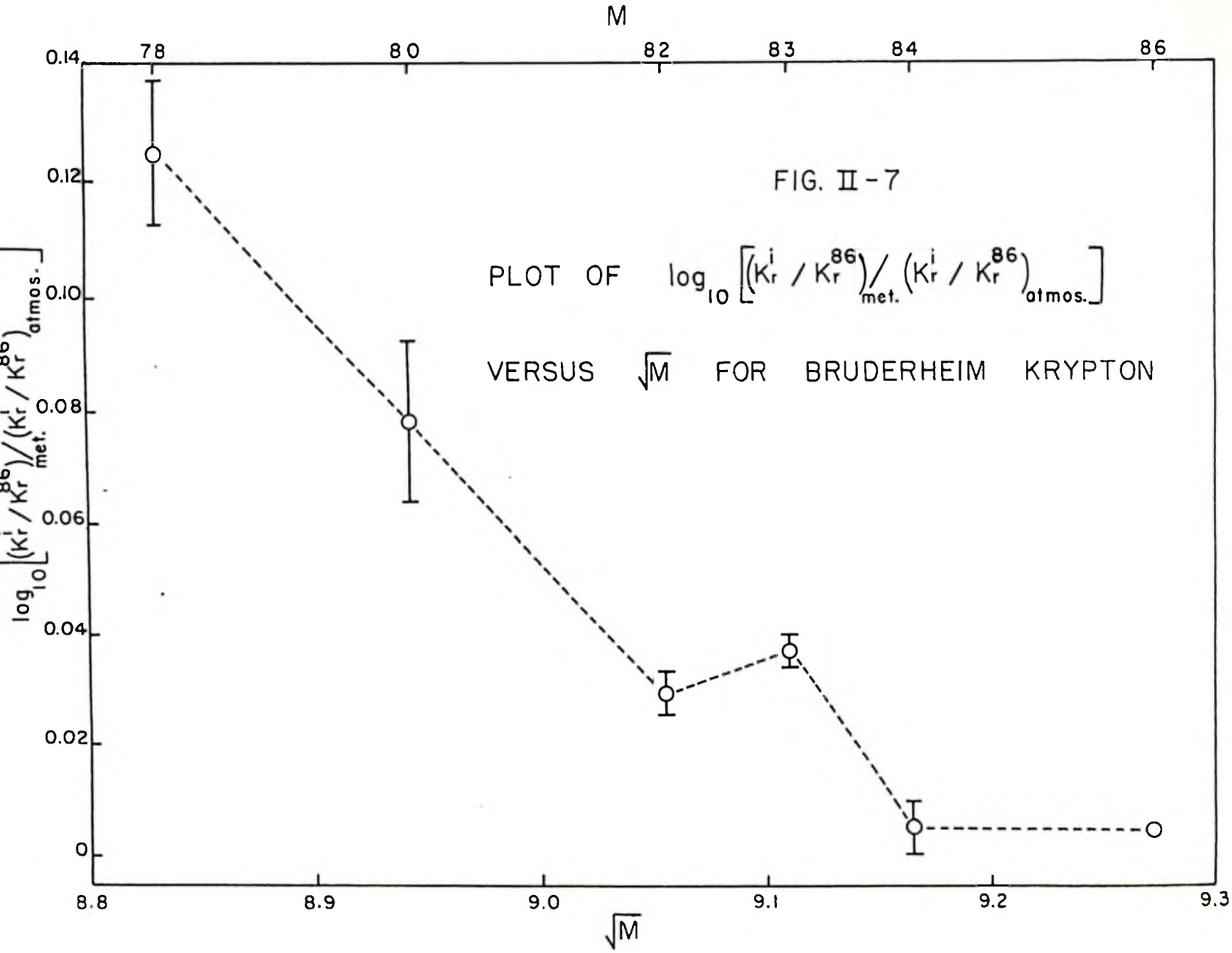

FIG. II-7

PLOT OF $\log_{10}\left[\left(K_r^i / K_r^{86}\right)_{met.} / \left(K_r^i / K_r^{86}\right)_{atmos.}\right]$

VERSUS $\sqrt{M}$ FOR BRUDERHEIM KRYPTON

anomalies in $Xe^{131-136}$ cannot have been caused by mass fractionation of either atmospheric xenon or natural gas xenon since no anomalies were observed for the shielded isotopes, within the errors of the isotope abundance measurements.

It will be shown later that most of the fission-product xenon in natural gas is from spontaneous fission of U^{238}. For the present, it may be noted that the presence of fission-product xenon in natural gas implies that most of the helium associated with it is evolved from U^{238} (and Th^{232}). If this assumption is correct, then there should be a good correlation between the ratio of helium to fission-product xenon and the ratio calculated from the decay parameters of uranium and thorium.

For a time period short compared to the radioactive half-lives of U^{238} and Th^{232}, and the spontaneous fission half-life of U^{238}, the following relationships are obtained:

$$\text{Radiogenic helium} = He_{rad} \propto C(U) \frac{T}{T\alpha} \cdot 8 + C(Th) \frac{T}{T\alpha'} \cdot 6$$

$$\text{Fission-product xenon} = Xe_f \propto C(U) \frac{T}{T_f} \cdot Y$$

where C(U) and C(Th) are concentrations of uranium and thorium

T is the age of the deposit

$T\alpha$ is the half-life of U^{238} for α-decay

$T\alpha'$ is the half-life of Th^{232} for α-decay

T_f is the half-life of U^{238} for spontaneous fission

Y is the yield of the xenon isotopes in spontaneous fission of U^{238}.

If we assume that C(Th)/C(U) = 4, the ratio He_{rad}/Xe_f is found to be 2×10^8. In the above calculation the values of T_α, T_α', T_f and Y used are 4.51×10^9 years, 1.39×10^{10} years, 8.3×10^{15} years and 0.16 respectively. The value of 2×10^8 may be compared with the experimental values for the ratio listed in Table II-XIII. The experimental values are seen to be uniformly higher than the theoretical value by about a factor of 2; a possible explanation for this is that the lighter gas, helium, diffuses more readily into natural gas than xenon.

The ratio of radiogenic argon to fission-product xenon is a useful parameter since it should be related to the potassium-uranium ratio in the rock reservoir by the equation

$$\frac{A_{rad}}{Xe_f} = \frac{T_f}{T_K} \cdot \frac{1}{Y} \cdot a \cdot \frac{C(K)}{C(U)} \cdot \frac{238}{40}$$

$$= 2.8 \times 10^3 \frac{C(K)}{C(U)}$$

where T_f is the half-life of U^{238} for spontaneous fission

T_K is the partial half-life of K^{40} for K-capture

Y is the yield of the xenon isotopes in spontaneous fission of U^{238}

a is the abundance of K^{40} in natural potassium

C(K) is the concentration of potassium

and C(U) is the concentration of uranium.

The same values of T_f and Y are used as in the previous calculation. The values taken for T_K and a are 1.3×10^{10} years and 0.000119 respectively. Assuming values of 3% for C(K) and 3 ppm for C(U) and inserting these values into the above equation yields

$$\frac{A_{rad}}{Xe_f} = 2.8 \times 10^7$$

TABLE II-XIII

The Ratios He_{rad}/Xe_f and A_{rad}/Xe_f for Natural Gas

Source	He_{rad}/Xe_f	A_{rad}/Xe_f
Panoma	.....	.....
Channing	3.2×10^8	3.4×10^7
Cliffside	5.8×10^8	4.4×10^7
Navajo	4.7×10^8	4.8×10^7

The good agreement between this value and the values of A_{rad}/Xe_f listed in Table II-XIII confirms the suggestion that the radiogenic gases in natural gas have been derived from a rock reservoir containing "normal" amounts of potassium and uranium (Wasserburg et al 1957; Zartman et al 1961).

2. The Fission Anomalies

Fig. II-8 shows a comparison of the fission yields of $Xe^{131-136}$ in Navajo natural gas with the yields in spontaneous fission of U^{238} (Ashizawa and Kuroda 1957; Young and Thode 1960). It is seen that there are marked discrepancies at masses 131 and 132. Although contributions from spontaneous fission of U^{235} and Th^{232} can be ruled out because of the long half-lives of U^{235} and Th^{232} for spontaneous fission, it is possible that the high yields at Xe^{131} and Xe^{132} relative to the U^{238} spontaneous fission pattern are caused by neutron-induced fission of U^{235}. This seems highly unlikely for the following reasons:

1. The yield of Xe^{132} (relative to Xe^{136}) in the fission-product xenon found in natural gas is higher than the yield of Xe^{132} (relative to Xe^{136}) in neutron-induced fission of U^{235}. Hence the fission yields observed for the fission-product xenon in natural gas cannot be obtained by assuming a combination of U^{238} spontaneous fission and U^{235} neutron fission.

2. Young and Thode (1960) have shown that the percentage of neutron-induced fission in uranium minerals reaches negligible proportions for minerals or ore concentrates containing less than 10% uranium. These findings have been confirmed by Hitoshi Sakai (1961). Hence, one would

FIG. II-8

COMPARISON OF FISSION YIELDS OF THE FISSION-PRODUCT COMPONENT OF XENON IN NATURAL GAS WITH THE YIELDS IN SPONTANEOUS FISSION OF U^{238}.

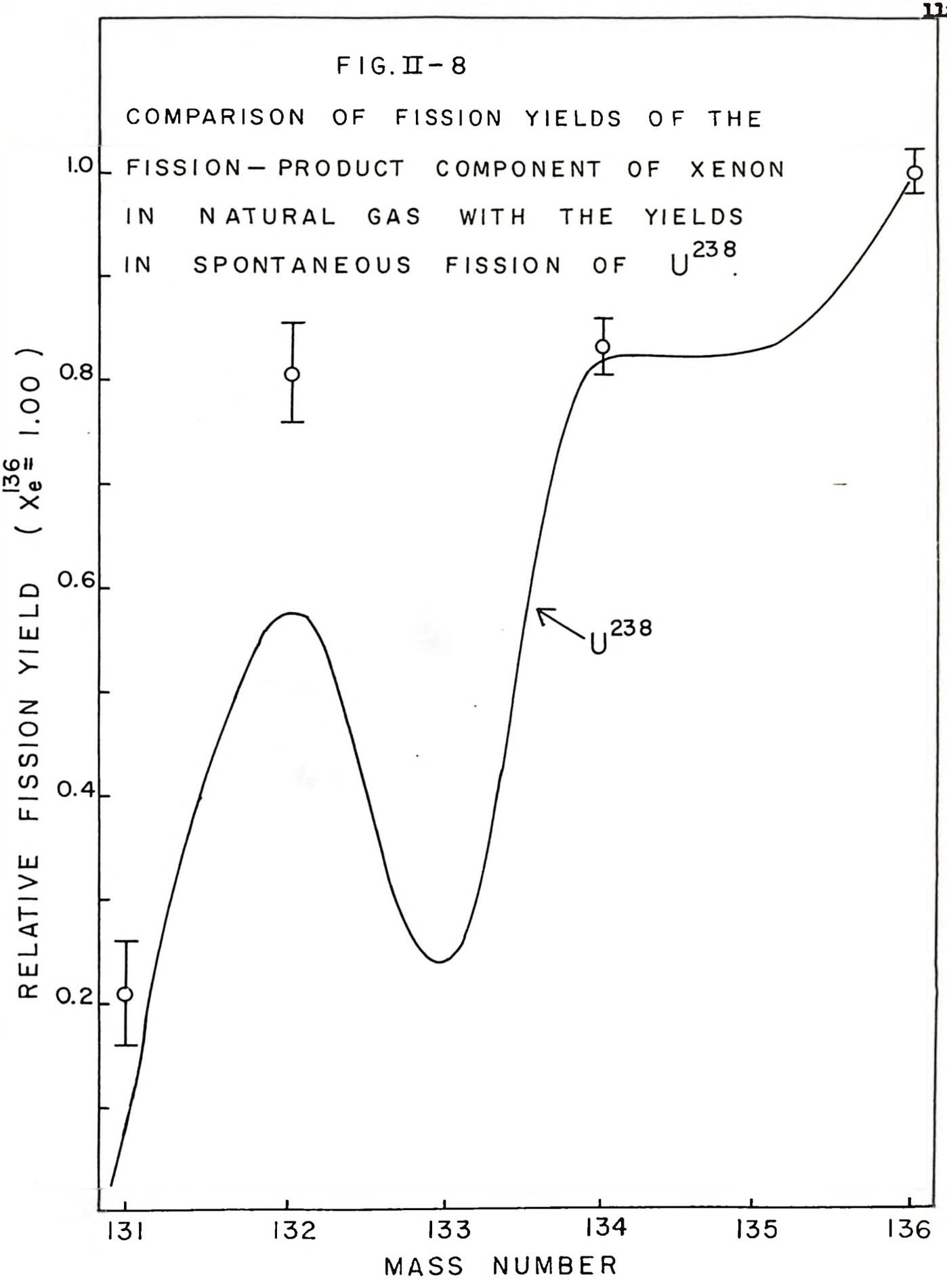

expect that spontaneous fission of U^{238} would predominate over neutron-induced fission of U^{235} in a "normal rock" reservoir containing only 3 ppm uranium.

The xenon yields in spontaneous fission of U^{238} have been accurately determined, and it has been shown that spontaneous fission of U^{238} must be largely responsible for the inventory of fission-product xenon in natural gas. Therefore, there can be little doubt that the discrepancies at Xe^{131} and Xe^{132} are real. These discrepancies can be well explained by analogy with the results obtained for low temperature ($< 500^{\circ}C$) diffusion of fission-product xenon from various uranium oxide powders. At such temperatures, only a small fraction of the available fission-product xenon had diffused from the powders. Hence it is likely that only a small fraction of the available fission-product xenon (and hence only a small fraction of the available radiogenic helium and argon) has diffused into natural gas from the surrounding rocks.

The discrepancies at Xe^{131} and Xe^{132} found for fission-product xenon (from Pu^{244}) in the earth's atmosphere (see Fig. II-6) are of course less certain owing to the lack of fission yield data for spontaneous fission of Pu^{244}. However, it would appear that there are two cases in nature where discrepancies are observed at Xe^{131} and Xe^{132} in fission-product xenon. In both cases the discrepancies can be explained by the mechanism of diffusion and decay of xenon precursors (see Part I).

Kuroda's hypothesis, that atmospheric xenon contains fission-product xenon from the spontaneous fission of Pu^{244}, has been criticised because of the large yield discrepancies at Xe^{131} and Xe^{132}. The above explanation of these discrepancies would seem to support Kuroda's hypothesis.

APPENDIX A

CALCULATION OF THE Xe^{133}/Xe^{135} ATOM RATIO

Sullivan (1957) gives the following data for the 133 and 135 mass chains:

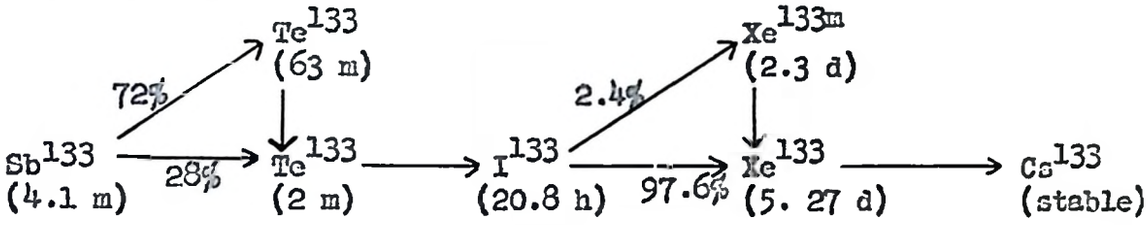

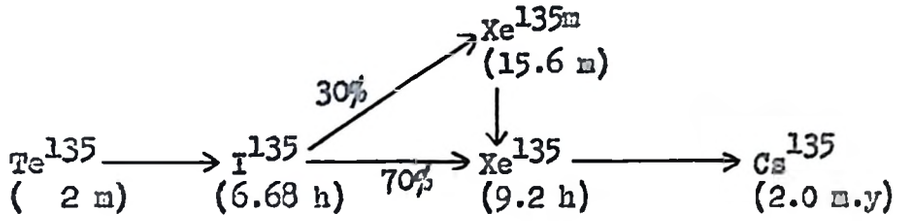

The irradiation time and cooling time involved in the Xe^{133}-Xe^{135} experiment were such that the entire 133 and 135 chains can be assumed to start at I^{133} and I^{135} respectively. Each chain may be represented by the following:

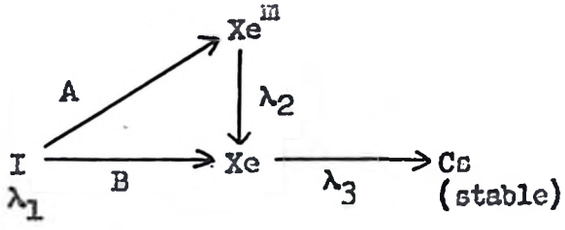

The number of atoms of xenon present at the time of analysis is given by:

$$N(Xe) = AR(f - g)h + \left[BR(a - b) + A(c - d) + \left\{\frac{1}{\lambda_2\lambda_3} + \frac{\lambda_1}{\lambda_2(\lambda_2 - \lambda_1)(\lambda_3 - \lambda_2)} - \frac{1}{(\lambda_2 - \lambda_1)(\lambda_3 - \lambda_1)}\right\} e\right] \exp(-\lambda_3 t_1)$$

where $a = (1 - \exp(-\lambda_1 T)) \exp(-\lambda_1 t)$

$$b = \frac{\lambda_1(1 - \exp(-\lambda_3 T)) \exp(-\lambda_3 t)}{\lambda_3(\lambda_3 - \lambda_1)}$$

$$c = \frac{(1 - \exp(-\lambda_1 T)) \exp(-\lambda_1 t)}{(\lambda_2 - \lambda_1)(\lambda_3 - \lambda_1)}$$

$$d = \frac{\lambda_1(1 - \exp(-\lambda_2 T)) \exp(-\lambda_2 t)}{\lambda_2(\lambda_2 - \lambda_1)(\lambda_3 - \lambda_2)}$$

$$e = (1 - \exp(-\lambda_3 T)) \exp(-\lambda_3 t)$$

$$f = \frac{(1 - \exp(-\lambda_1 T)) \exp(-\lambda_1 t)}{\lambda_2 - \lambda_1}$$

$$g = \frac{\lambda_1(1 - \exp(-\lambda_1 T)) \exp(-\lambda_2 t)}{\lambda_2(\lambda_2 - \lambda_1)}$$

$$h = \frac{\lambda_2}{\lambda_3 - \lambda_2} (\exp(-\lambda_2 t_1) - \exp(-\lambda_3 t_1))$$

R is the fission rate multiplied by the fractional yield of the 133 or 135 mass chains

T is the irradiation time

t is the cooling time between irradiation and extraction

t_1 is the cooling time between extraction and analysis

The yield ratio of the 133 and 135 mass chains was taken to be 1.026 (Farrar and Tomlinson 1962). The cooling time t was taken to be the time interval between the end of irradiation and the end of the 3-hour constant temperature heating period.

The cooling time t_1 was taken to be the time interval between the end of the 3-hour constant temperature heating period and the time of analysis.

APPENDIX B

THE I^{129}-Xe^{129} DECAY INTERVAL

Suppose that I^{129} and I^{127} are produced at constant rates K_{129} and K_{127} during a time T. At the end of time T the I^{129}-I^{127} ratio is given by:

$$\frac{I^{129}(T)}{I^{127}(T)} = \frac{\tau K_{129}}{T K_{127}} \left[1 - \exp\left(-\frac{T}{\tau}\right) \right]$$

where τ = the mean life of I^{129}.

For $\tau \ll T$, the above equation reduces to

$$\frac{I^{129}(T)}{I^{127}(T)} = \frac{\tau}{T} \frac{K_{129}}{K_{127}}$$

Suppose that after a further time interval Δt, Xe^{129} formed from decay of I^{129} is retained. The total Xe^{129} present after complete decay of I^{129} is given by:

$$\frac{I^{129}(T + \Delta t)}{I^{127}(T + \Delta t)} = \frac{\tau}{T} \frac{K_{129}}{K_{127}} \exp\left(-\frac{\Delta t}{\tau}\right) = \frac{Xe^{129}{}_r}{I^{127}(T + \Delta t)}$$

If it is assumed that $I^{127}(T + \Delta t)$ is equal to the present content of I^{127}, then the following expression is obtained:

$$\ln\left(\frac{I^{127}}{Xe^{129}_r}\right) = \frac{\Delta t}{\tau} + \ln\left(\frac{T}{\tau}\right) + \ln\left(\frac{K_{127}}{K_{129}}\right)$$

Δt for the meteorites represents the time interval between the cessation of nucleosynthesis of duration T, and the retention of radiogenic Xe^{129} in the meteorite.

BIBLIOGRAPHY

Anders, E. 1962. Rev. Mod. Phys. 34, 2, 287.

Ashizawa, F. T. and Kuroda, P. K. 1957. J. Inorg. Nucl. Chem. 5, 12.

Barrer, R. M. 1941. Diffusion in and Through Solids. Cambridge University Press.

Belle, J. 1959. Proceedings of the Second United Nations Conference on the Peaceful Uses of Atomic Energy 6, 569, United Nations, Geneva.

Booth, A. H. and Rymer, G. T. 1956. AECL Report PR-CM-7.

Booth, A. H. 1957. CRDC-721, AECL Report No. 496.

Booth, A. H. and Rymer, G. T. 1958. CRDC-720, AECL Report No. 692.

Boyd, G. E., Adamson, A. N. and Myers, L. S., Jr. 1947. J. Amer. Chem. Soc. 69, 2836.

Brown, H. 1947. Phys. Rev. 72, 348.

Clarke, W. B. and Thode, H. G. 1961. J. Geophys. Research 66, 3578.

Damon, P. E. and Kulp, J. L. 1958. Geochim. et Cosmochim. Acta, 13, 280.

Farrar, H. and Tomlinson, R. H. 1962. Nuclear Physics 34, 2, 367.

Festa, C. and Santangelo, M. 1952. Ann. geofis (Rome) 3, 489.

Goles, G. G. and Anders, E. 1961. J. Geophys. Research 66, 889.

Goles, G. G. and Anders, E. 1962. Geochim. et Cosmochim. Acta. In Press.

Jeffery, P. M. and Reynolds, J. H. 1961. J. Geophys. Res. 66, 3582.

Kennett, T. J. and Thode, H. G. 1956. Phys. Rev. 103, 323.

Kennett, T. J. and Thode, H. G. 1960. Can. J. Phys. 38, 945.

Khlopin, V. G., Gerling, E. K. and Baranovskaya, N. V. 1947. Bull. Acad. Sci. U.R.S.S., Classe Sci. Chim. 599.

Khlopin, V. G. and Gerling, E. K. 1948. Doklady Akad Nauk. S.S.S.R. 58, 1415.

Krummenacher, D., Merrihue, C. M., Pepin, R. O. and Reynolds, J. H. 1962. Geochim. et Cosmochim. Acta 26, 231.

Kuroda, P. K. 1960. Nature 187, 36.

Levis, W. B. 1960. AECL Report DM58.

Lindner, R. and Matzke, H. 1959. Z. Naturforsch. 13a, 794.

Macnamara, J. and Thode, H. G. 1950. Phys. Rev. 80, 471.

Markowitz, J. M., Koch, R. C. and Roll, J. A. 1957. Bettis Report WAPD-180.

Nier, A. O. 1950. Phys. Rev. 79, 450.

Reichenberg, D. 1953. J. Amer. Chem. Soc. 75, 589.

Reynolds, J. H. 1960a. Phys. Rev. Letters 4, 4.

Reynolds, J. H. 1960b. Phys. Rev. Letters 4, 351.

Reynolds, J. H. 1960c. J. Geophys. Research 65, 3843.

Reynolds, J. H. 1960d. Z. Naturforsch. 15a, 1112.

Sakai, Hitoshi. 1961. Unpublished work in this laboratory.

Sakakura, A. Y., Lindberg, C. and Paul. H. 1959. U.S.G.S. Bull. 1052-I, 287.

Signer, P. 1960. Z. Naturforsch. 15a, 748.

Steinberg, E. P. and Glendenin, L. E. 1954. Phys. Rev. 95, 431.

Steinberg, E. P. and Glendenin, L. E. 1955. J. Inorg. Nucl. Chem. 1, 45.

Sullivan, W. H. 1957. Trilinear Chart of the Nuclides.

Thode, H. G. and Graham, R. L. 1947. Can. J. Research 25A, 1.

Turekian, K. K. 1959. Geochim. et Cosmochim. Acta 17, 37.

Urey, H. C. 1952. The Planets. Yale University Press, New Haven, Conn.

Wanless, R. K. and Thode, H. G. 1955. Can. J. Phys. 33, 541.

Wasserburg, G. J., Czamanske, G., Faul, H. and Hayden, R. J. 1957. Nat. Acad. Sci., Nat. Res. Council Pub. 572. Nuclear Science Series Report No. 23, 156.

Wasserburg, G. J., Fowler, W. A. and Hoyle, F. 1960. Phys. Rev. Letters 4, 112.

Yaffe, L. and Macintosh, C. E. 1947. Can. J. Research 25B, 371.

Young, B. G., Kennett, T. J. and Thode, H. G. 1957. Unpublished work in this laboratory.

Young, B. G. 1958. PhD. Thesis, McMaster University.

Young, B. G. and Thode, H. G. 1960. Can. J. Phys. 38, 1.

Zahringer, J. and Gentner, W. 1961. Z. Naturforsch. 16a, 239.

Zartman, R. E., Wasserburg, G. J. and Reynolds, J. H. 1961. J. Geophys. Research 66, 277.